Climate Dynamics (2021) 56:3749–3773
https://doi.org/10.1007/s00382-021-05665-4

Possible impact of equatorially trapped waves on the tropical cyclone drift

Hyun-Geun Shin[1] · **Boualem Khouider**[1]

Received: 11 July 2020 / Accepted: 19 January 2021 / Published online: 1 February 2021

Abstract
The effect of equatorially trapped waves on the movement of tropical cyclones (TC) is studied numerically based on a two-dimensional barotropic model in a beta-plane approximation. According to recent studies, equatorially trapped waves contribute to the genesis of TCs. It is thus natural to assume that these waves affect also the movement of the TC. The effect of three types of equatorially trapped waves, namely Kelvin, Rossby, and n = 0 eastward inertio-Gravity (EIG) waves, on the TC trajectory is investigated with a focus on the sensitivity on some key physical parameters such as the wavenumber and wavespeed. Using a simple barotropic model forced by a prescribed baroclinic flow, the barotropic response to equatorially trapped waves is simulated for a period of 50 days, under various wave parameter configurations. This response is then used as a background flow where TC's can evolve and propagate. TC-like flows are injected into this wavefield background at arbitrary times during the simulation, and the TC trajectories are tracked and recorded for 48h after the injection time. The resulting TC trajectory patterns with respect to the injection times and wave parameters appear to be stochastic and the mean paths and the associated standard deviations are calculated and reported here. The statistics are different for different wave types. Kelvin waves make shorter length of TC trajectories and small divergence of direction. On the contrary, Rossby waves cause rather dramatic changes in the TC path and yield longer trajectories. Meanwhile, TCs in EIG waves maintain fairly the same direction and typically have longer trajectories though less dramatic. A robustness test using a random forcing instead has also been conducted.

Keywords Tropical cyclone drift · Barotropic model · Equatorially trapped waves

1 Introduction

The movement of tropical cyclones (TCs) has been investigated for decades. It is found that the so-known beta gyres that form because of the interaction of the TC with earth's curvature due to its rotation, make TCs move northwestward, through the advection of planetary vorticity by these gyres. This phenomenon is known as the beta drift.

Fiorino et al. (1989) have systematically examined the effect of the TC wind profile on its movement using a non-divergent barotropic model without a background flow. By artificially altering different parts of the TC wind profile, they concluded that the effect of the outer wind profile is the most significant. Ross and Kurihara (1991) simulated the asymetric flow generated by the beta-effect in a barotropic flow. Li and Wang (1994) investigated the dynamics of the beta gyre and TC drift using a shallow-water model. Using three different wind profiles, they tried to understand the physical processes related to the beta gyres. They analyzed the beta effect in terms of energy and concluded that the beta drift is responsible for energy transfer.

The beta gyres take the kinetic energy of the symmetric circulation of the TC to produce asymmetric circulations, which is called beta conversion or nonlinear conversion. The same authors performed a three-dimensional numerical study of the beta drift, and found that the meridional speed of TC's is proportional to the angular momentum (Wang and Li 1992). Meanwhile, Smith (1993) devised an analytical theory for the movement of TC's based on a barotropic model. The theory's predictions of the motion of TC's are in good agreement with the results from an equivalent numerical model (Smith 1993).

✉ Boualem Khouider
khouider@uvic.ca

[1] Department of Mathematics and Statistics, University of Victoria, Victoria, BC, Canada

Chan and Williams (1987) investigated the beta effect on the movement of TC's while they also tried to understand the effect of a background zonal flow on the TC movement. This work led to a more general line of research on the interactions between TCs and the environmental flow (Williams and Chan 1994). The results in Williams and Chan (1994) suggest that with a nonlinear barotrpic model, the direction of the zonal mean flow influences the traveling distance of the TC rather than its traveling direction. A TC moves longer in an eastward flow background when the magnitude of the wavenumber one (asymmetric) flow is the highest. This means that the beta conversion of energy is the largest in an eastward flow background condition; In the special case of a parabolic jet, the traveling distance is not very much affected but the TC direction depends strongly on the wind direction. A cyclone moves further poleward in an eastward flow background and more so when the magnitude of wavenumber one flow is the highest.

Moreover, the interaction of TCs with non-divergent wave-like flows are studied in Demaria (1985). The aforementioned works are helpful to understand the crucial factors of the background flow that influence the track of TC's but they are based on simple flows which may or may not occur in the atmosphere. More recently, Huang et al. [9] used numerical simulations to study the impact of a mountain range on the TC trajectories.

According to studies of cyclo-genesis, TCs are formed by and nested within various types of atmospheric waves. Schreck III et al. (2012) studied the contribution of equatorially trapped waves to the occurrence of TC's over the globe. The contribution of different waves differs from region to region, but tropical depressions (TD) are found to be the main influential entity in the Northern Hemisphere. Equatorial Rossby (ER) waves are found to be the second important factor, but the contributions of TD and ER waves are similar in the Southern Hemisphere. Kelvin waves are found to be of greatest influence in the North Indian Ocean, but they have the lowest contribution to cyclo-genesis overall. MRG waves have been reported to play a role in TC genesis (Shen et al. 2012) in the same way as African Easterly waves, which are known to provide the mother vortex for Hurricanes in the tropical Atlantic (Shen 2019; Shen et al. 2010a, b).

Reynolds et al. (2016) found a connection between Kelvin waves and TC activity. Over the Indian Ocean, an infrared image indicates that TC's energy conversion is enhanced during the passage of a Kelvin wave. The same phenomenon occurs for a tropical storm. Their energy sensitivity tests show that the precursor of a tropical cyclone is sensitive to the initial Kelvin wave disturbance. Zhao and Liguang (2018) examined the formation frequency of TC's in the Western North Pacific in connection with ER waves. They found a strong relationship between the frequency of TCs and ER waves and that the genesis area is shifted to the region of active convection associated with ER waves. Zhou and Wang (2007) found that upper tropospheric mixed Rossby gravity (MRG) waves develop MRG circulation in the lower troposphere, thereby a TD-type disturbance takes place (Zhou and Wang 2007). These are corroborated by the work of Shen et al. (2012). While these studies have dealt with one single type of waves, Chen and Chou (2014) considered the joint contribution of multiple equatorial waves to the cyclo-genesis over the Western North Pacific. They demonstrated that the potential of cyclo-genesis due to multiple waves is larger than that of a single wave.

Kiladis et al. (2009) provides a comprehensive review about convectively coupled equatorial waves (Kiladis et al. 2009). Kelvin waves in the tropics move eastward and have short-lived convective cells embedded in synoptic-scale envelopes associated with largely cloud-covered areas characterized with upward motions. They are sometime themselves embedded within the Madden–Julian Oscillation (MJO), the dominant mode of variability in the tropical atmosphere on the intra-seasonal scale (Khouider 2019).

The relationship between cloudiness and both dynamical and thermodynamical fields of Kelvin waves differs with regions. The wavelength is reported to have 10,000 km or much shorter. Kelvin waves propagate with different wave speed in different areas. According to the observation over the Indian Ocean, the wave speed is from 12 to 15 m s^{-1}, but it could be slower through the MJO (Roundy and Frank 2004). Rossby waves move westward and have symmetric cyclonic circulations on both sides of the equator. The cyclone structures in one case study are propagating at speed of around 4.5 m s^{-1}. The slow speed and broad spatial scales allow them to be modulated when propagating through varying background wind states. They have a barotropic structure which means that they are only weakly coupled to convection, but a more complex vertical structure is observed when deep convection takes place. The structure of Rossby waves varies seasonally and regionally. The variability decreases from West to East across the Pacific. MRG waves develop hybrid structures with some disturbances especially over the Western Pacific. In the Central Pacific, gyres on the equator correspond to eastward propagating MRG waves, also known as $n = 0$ eastward inertio-gravity (EIG) waves (Kiladis et al. 2009). They become off-equatorial gyres which propagate northward toward the Philippines. Relatively fast MRG waves usually exist in the upper troposphere and the lower stratosphere, and show large perturbations in the lower troposphere. Over the Western Pacific, it is reported by Roundy and Frank (2004) that MRG waves propagate westward at speeds varying from 15 to 25 m s^{-1}. The wavelength was measured to be around 9000 km.

In this paper, the effect of equatorially trapped waves, namely Kelvin, Rossby and $n = 0$ EIG wave, on the movement of TCs is numerically investigated. It has to be noted that among the westward and eastward propagating MRG waves, we choose to study the effect of n = 0 EIG (or eastward MRG) waves because of their ubiquity in the Central Pacific in conjunction with Kelvin and Rossby waves which are predominant in the Indian ocean and Western Pacific. Westward propagating MRG's are abundant in both the Western and Central pacific basins (Kiladis et al. 2009) but arguably their flow structure and propagation characteristics are reminiscent to those of Rossby waves. In the reminder of this article we use the term MRG wave to refer to n = 0 EIG MRG-type waves, used in this study. The present study is by no means comprehensive. It is meant only as an illustration of the fact that equatorial waves of certain type may significantly influence the path of TC's while others may not.

We use a non-divergent barotropic model in an equatorially centred periodic channel forced by a prescribed baroclinic flow. Using equatorially trapped waves as the main forcing, the barotropic flow response is simulated for a period of 50 days, starting with a vanishing initial condition. A TC-like flow is injected into the wave-induced barotropic background at an arbitrary time during the simulation and the TC trajectory is tracked and recorded. The same experiment is then repeated with varying TC injection times and various equatorially trapped wave types and wave parameters, namely, the wavenumber and wave speed. The wavenumber in particular determines the wavelength scale and may have a strong influence on the barotropic flow response and consequently on the TC path. The dependence of the results on the injection time seems to be stochastic. The associated patterns are thus identified and analyzed by calculating the mean paths and the associated standard deviations. Nonetheless, the stochasticity seems to be controlled by the wave phase in which the TC is injected while the wave-type itself seems to have a deterministic impact on the TC path. To illustrate this point, we have performed a robustness test where the wave-forcing is replaced by a correlated noise that varies in both time and space, mimicking a source of energy backscatter from unresolved turbulence, used in weather prediction models (Berner et al. 2009).

The paper is organized as follows. The model equations and the computational setup are described in Sect. 2. The main results and discussion are presented in Sect. 3, including the robustness test using an energy backscatter–correlated noise as a forcing mechanism while a conclusion is given in Sect. 4.

2 Model equations and computational setup

2.1 Governing equations: barotropic flow forced by equatorially trapped waves

Following Khouider and Majda (2000), the derivation of the simple barotropic and baroclinic models for TCs and equatorially trapped waves, respectively, is based on a Galerkin projection of the equatorial-beta-plane non-linear primitive equations onto the barotropic and first baroclinic modes of vertical structure (Kasahara and Puri 1981; Majda 2003; Khouider et al. 2013; Khouider 2019). More details on the derivation and the use of these models to study various aspect of equatorial wave dynamics and precipitation fronts can be found in Frierson et al. (2004), Biello and Majda (2004), Khouider and Majda (2000), Khouider and Majda (2005), Ferguson et al. (2009), Khouider et al. (2013). This Galerkin projection results in two shallow water-like systems representing the barotropic and baroclinic flow components that are nonlinearly coupled through the associated cross advection terms.

When the baroclinic equations are ignored, we obtain a system of non-divergent barotropic equations forced by a prescribed baroclinic flow, that are used here to simulate the movement of a TC-like flow. The forced barotropic equations take the form

$$\frac{\partial \bar{\mathbf{v}}}{\partial t} + \bar{\mathbf{v}} \cdot \nabla \bar{\mathbf{v}} + y\beta \bar{\mathbf{v}}^{\perp} + \nabla \bar{p} = -\frac{1}{2}(\mathbf{v} \cdot \nabla \mathbf{v} + \mathbf{v} \nabla \cdot \mathbf{v}), \qquad (1)$$

where $\bar{\mathbf{v}}$ and $\bar{\mathbf{p}}$ are respectively the velocity and pressure fields of the barotropic flow while $\mathbf{v}$ is the baroclinic velocity vector, which is assumed to be prescribed in this study. Here $\nabla = (\partial_x, \partial_y)$ is the horizontal gradient operator where x is the East-West—along-the-equator coordinate and y is the signed distance from the equator (positive to the north and negative to the south) while $\beta = 2.2804 \times 10^{-11}\,\mathrm{s}^{-1}\mathrm{m}^{-1}$ is the y-gradient of the Coriolis parameter. The terms on the right hand side represent the forcing by a prescribed first baroclinic flow where $\mathbf{v}$ is the first baroclinic velocity vector.

For simplicity, the barotropic equations are rewritten in vorticity-stream function form,

$$\frac{\partial \xi}{\partial t} + \bar{u}\frac{\partial \xi}{\partial x} + \bar{v}\frac{\partial \xi}{\partial y} + \beta \bar{v} = -\frac{1}{2}\left[\left(\frac{\partial^2}{\partial x^2} - \frac{\partial^2}{\partial y^2}\right)(uv) + \frac{\partial^2}{\partial x \partial y}(v^2 - u^2)\right]. \qquad (2)$$

Here, $\bar{u}$ and $\bar{v}$ are respectively the x and y barotropic velocity components and $\xi = \partial_x \bar{v} - \partial_y \bar{u}$ is the associated relative vorticity. Accordingly, u and v are respectively the x and y baroclinic velocities.

In the numerical simulations reported below, the equations in (1) to (2) are non-dimensionalized based on the equatorial synoptic dynamics where the first baroclinic gravity wave speed $c_0 = 50$ m s^{-1} is used as the velocity scale, the equatorial Rossby deformation radius $L_e = (c_0/\beta)^{1/2} \approx 1500$ km is the length scale, and $T = (c_0\beta)^{-1/2} \approx 8.33$ h is the time scale (Majda 2003; Frierson et al. 2004; Khouider and Majda 2000; Biello and Majda 2004; Khouider et al. 2013; Khouider 2019). In these units both the β parameter and the gravity wave speed are unity.

2.2 Idealized equatorial wave forcing

Using Eq. (2), the time varying velocities u, v of three equatorially trapped waves are used as a prescribed forcing to produce a barotrobic flow background. Using this model, Ferguson et al. (2009) found that a prescribed Kelvin wave induces a strongly significant and complex barotropic flow consisting of a wave-locked large-scale wave-like response that moves eastward with the Kelvin wave and a sequence of Rossby waves that move in the opposite direction. Here, we are interested in the effect of such an induced barotropic flow on the evolution and movement of TC-like vortices.

Equatorially trapped waves play a major role in tropical weather and climate dynamics. They are associated with cloud super-clusters that account for the majority of the tropical atmosphere variability on synoptic scales, both in terms of fluid dynamics (wind, temperature) and rainfall (Kiladis et al. 2009; Khouider 2019). Their effective propagation speed vary with the geographic location and the degree of convective coupling as previously stated (Kiladis et al. 2009).

Before we dive into the detailed mathematical formulation of the type of equatorially trapped waves, we define their specific parameters that are considered during the study.

We introduce the wave magnitude A, defined as the wave velocity maximum, which we assume is fixed to $A = 15$ m s^{-1} throughout this study. This value is chosen as a benchmark maximum magnitude within the realm of upper tropospheric tropical baroclinic flows (Frierson et al. 2004). Below, we give the non-dimensional formulations of the wave flows used here for the sake of completeness, each followed by the dispersion relation written in the original units in terms of an equivalent gravity wave speed c_e, associated with a certain equivalent depth, which we vary as a parameter. While the flow fields are based on the dry dynamics exact solutions of the baroclinic equations corresponding to the imposed equivalent gravity wave speed, the induced variations in the wave speed are set to mimic the wide spectrum of speeds that are observed in nature (Roundy and Frank 2004; Roundy 2012). The other key parameter on which the wave flow structure strongly depends is the wavenumber, denoted by k in the present study. It sets the wavelength and thus the horizontal scale of the wave. Except for the Kelvin wave which is non-dispersive, the actual wave phase speed also depends on on the value of k.

Details on equatorially trapped waves, as special solutions for the equatorial beta-plane shallow water equations, can be found in many monographs, textbooks and review papers. See for example Khouider (2019), Kiladis et al. (2009), Majda (2003). The mathematical formulations of the flow velocity and dispersion relations of the equatorial waves utilized in this study are given next.

The Kelvin wave flow formulation and dispersion relation are given by

$$\begin{aligned} u &= A\exp(-y^2/2)\cos(kx - \omega t), \\ v &= 0, \\ \omega &= kc_e. \end{aligned} \tag{3}$$

The Kelvin wave in Eq.(3) moves eastward along the equator at the constant speed $c = c_e$ and its meridional structure decays exponentially fast, away from the equator. Since the

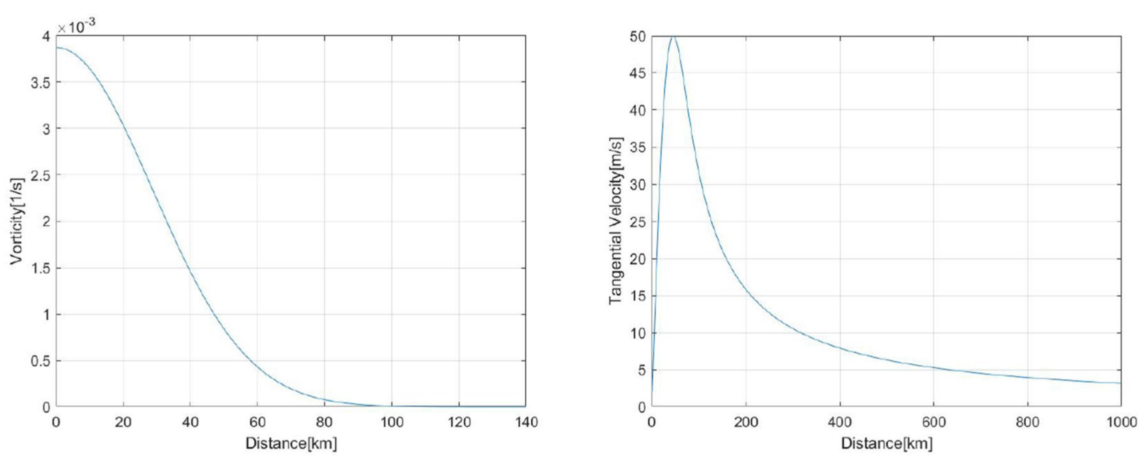

Fig. 1 The profile of the assumed vorticity distribution (left) of the TC at time t = 0 and the associated horizontal wind profile (right)

frequency (ω) is a linear function of wavenumber (k), Kelvin waves are said to be non-dispersive.

The Rossby wave formulation is given by

$$
\begin{aligned}
u &= A\frac{1}{2}\exp(-y^2/2)\sin(kx-\omega t)(\frac{2y^2-1}{k-\omega}-\frac{1}{k+\omega}),\\
v &= Ay\exp(-y^2/2)\cos(kx-\omega t),\\
\omega &= -\frac{c_e\beta k}{c_e k^2+(2n+1)\beta}.
\end{aligned}
\tag{4}
$$

Here, we consider only the symmetric Rossby wave with the largest meridional index $n = 1$. The velocity components u and v of the Rossby wave in Eq. (4) depend highly on the wavenumber and phase speed. Rossby waves are dispersive since the frequency is a nonlinear function of the wavenumber and they move westward.

The MRG wave is expressed by

$$
\begin{aligned}
u &= -A\omega y\exp(-y^2/2)\sin(kx-\omega t),\\
v &= A\exp(-y^2/2)\cos(kx-\omega t),\\
\omega &= 0.5kc_e+0.5\sqrt{k^2c_e^2+4c_e\beta}.
\end{aligned}
\tag{5}
$$

While MRG waves can move in both directions along the equator, depending on the sign of the wavenumber, here we focus on the eastward moving ones ($k > 0$) because they are significant in Eastern Pacific (Kiladis et al. 2009) while the Westward MRG waves have arguably a similar structure as Rossby waves and they both move westward. The eastward MRG waves are also called $n = 0$ eastward inertia-gravity or Yanai waves. MRG waves are also dispersive.

The wavenumber (k) and the effective gravity wave speed c_e are the wave parameters that are systematically varied here while the wave amplitude is fixed to the conservative value of $A = 15$ m s^{-1}. The actual wave speed for the three waves is given by the relation $c = \frac{\omega}{k}$, where ω is the frequency which is given in terms of the effective gravity wave

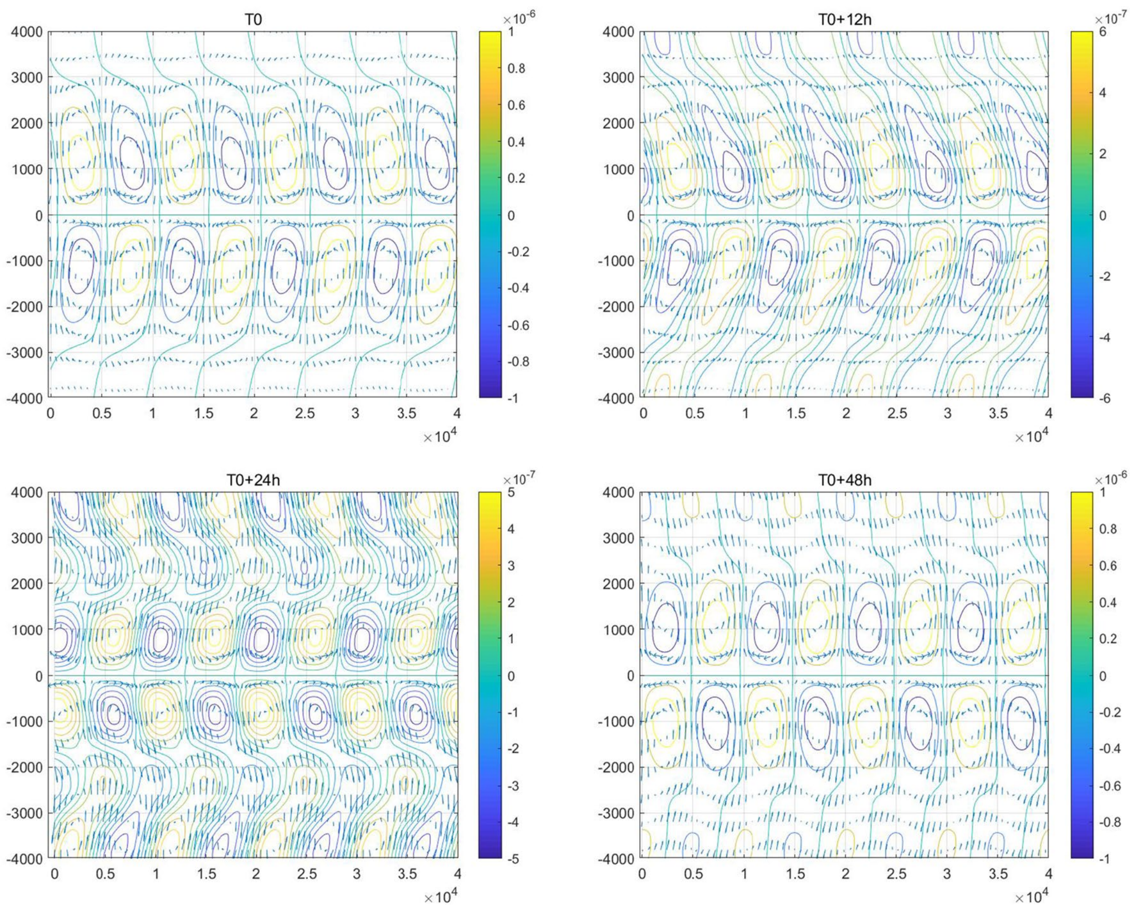

Fig. 2 Barotropic flow response to a Kelvin wave forcing at $T_0 = 10$ days, at T_0 + 12 h, at T_0 + 24 h, and at T_0 + 48 h. The wavenumber is $k = 5$, the phase speed is $c = 1$ m s^{-1} and the wave amplitude is $A = 15$ m s^{-1}. The contours of vorticity (s $^{-1}$) are overlaid by velocity vector arrows. The largest arrow corresponds to a maximum speed of 2.00 m s^{-1} at T_0, 1.98 m s^{-1} at T_0 + 12 h, 2.01 m s^{-1} at T_0 + 24 h, and 2.06 m s^{-1} at T_0 + 48 h

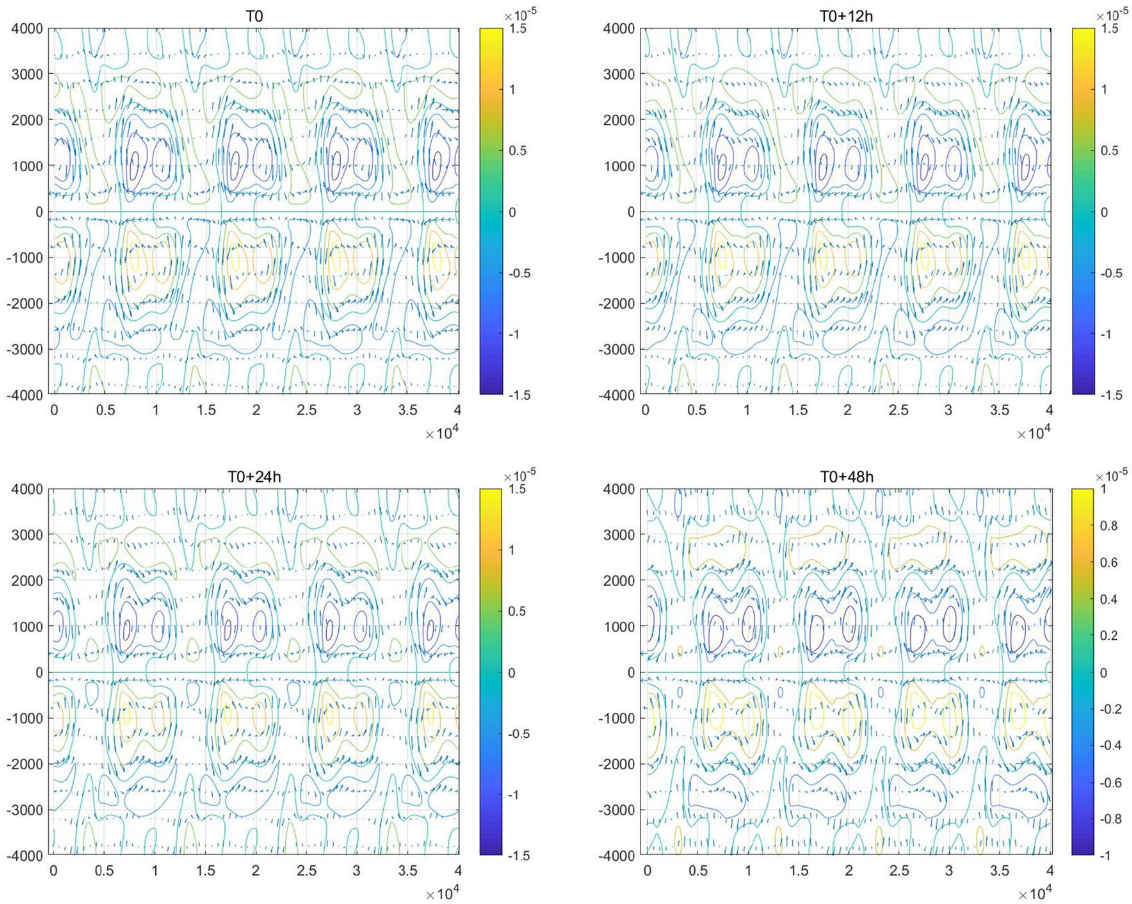

Fig. 3 Same as Fig. 2 but for the case of a Rossby wave forcing with $k = 1$ and $c = -0.332$ m s^{-1}. The largest arrow corresponds to a maximum speed of 14.52 m s^{-1} at T_0, 14.44 m s^{-1} at $T_0 + 12$ h, 14.27 m s^{-1} at $T_0 + 24$ h, and 9.73 m s^{-1} at $T_0 + 48$ h

speed c_e through the dispersion relations in (3) to (5). For the Kelvin wave, we have $c = c_e$ while in the other two cases c depends on both parameters k and c_e.

In the non-dimensional units, making the Rossby deformation number as the reference length scale, the factor $\exp(-y^2/2)$, which modulates the meridional structure of the equatorial waves in (3)–(5), marks the fact that these waves are trapped in the vicinity of the equatorial and decay exponentially fast away from the equator on that scale.

2.3 Tropical cyclone-like flow seeding

The structure of TCs has been investigated for a long time, and the general structure consists of an eye, an eyewall, and rainbands. In the eyewall, there is the strongest wind area, and the distance from the eye to this area is called the radius of maximum wind (RMW). In this study, the following exponential form (Li and Wang 1994) is adopted for the TC's vorticity distribution and is used as the initial TC seeding for all the numerical simulations presented here. We set

$$\xi(r) = \frac{\alpha}{L_e} \exp(-(r/L_r)^2), \tag{6}$$

as our idealized model for the TC's vorticity structure. Here, α is the TC magnitude, L_e is the Rossby deformation radius defined above, and L_r is the synoptic length scale of the TC. It is set to $L_r = 30$ km. This value is chosen in consideration of real data to represent a medium sized tropical cyclone (Stern et al. 2014). The associated profiles of vorticity and tangential velocity are shown in Fig. 1. Accordingly, the radius of maximum wind of the TC is fixed to 45 km, and the speed of the maximum wind is set to 50 m/s.

In the numerical experiments below, the tropical cyclone-like flow in (6) is added to the flow field generated by the barotropic equations in (2), when forced by one of the equatorial waves in (3)–(5), after an arbitrary spin up time $T_0 \geq 0$. The behaviour of the tropical cycle under the influence of equatorially tropical waves is thus analysed and investigated.

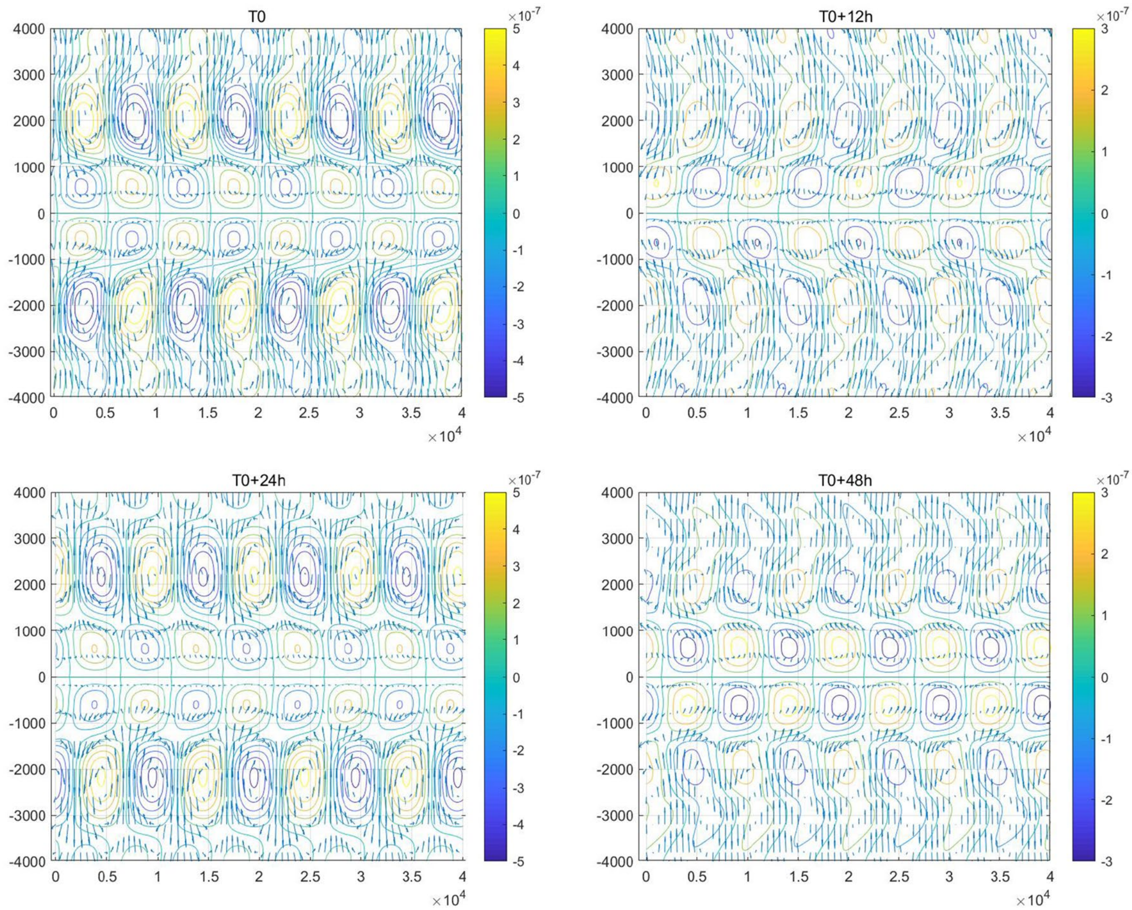

Fig. 4 Same as Fig. 2 but for the case of an MRG wave forcing with $k = 8$ and $c = 1.802$ m s^{-1}. The largest arrow corresponds to a maximum speed of 1.79 m s^{-1} at T_0, 1.74m s^{-1} at $T_0 + 12$ h, 1.73 m s^{-1} at $T_0 + 24$ h, and 1.80 m s^{-1} at $T_0 + 48$ h

2.4 Computational setup

Following Khouider and Majda (2000), the barotropic equations in (2) are solved numerically using a second order finite volume method combined with a semi-spectral solver for the Poisson equation connecting the stream function and the relative vorticity. The effect of the forcing on the right hand side is integrated exactly based on a time-splitting strategy. The interested reader is referred to Khouider and Majda (2000) for the details.

The computational domain is a rectangular channel of 40,000 km in the x-direction and 16,000 km in the y-direction, centred at the equator. The grid mesh size is 20 km and uniform in both directions. Preliminary tests where three grid resolutions of 10 km, 20 km, and 40 km revealed that, for the type (size and shape) of tropical cyclone like disturbance used here, as in (6) and Fig. 1, a mesh size of 20 km provides a good balance between accuracy and efficiency of the simulations (Hyun-Geun 2019). The initial location of the TC centre (point of maximum vorticity) is set at 20,000 km in the x-direction (in the middle) and to 800 km in the y-direction (north of the equator). The boundary conditions are periodically symmetric in x and a no-flow condition is used in y, i.e, $v = 0$ at the north and south channel walls. The duration of the TC simulations is 2 days, and the data is saved every 6 h. Preliminary tests, without a background flow, showed that the two-day simulation period is long enough for the injected disturbance to move a significant distance while it reasonably maintains its overall TC-like shape.

As already mentioned, to determine the effect of the equatorial waves on the TC movement, we proceed as follows. We solve the equations in (2) using the above numerical set up with the forcing on the right hand side determined by one of the wave solutions in (3) to (5) and with homogeneous initial condition $\bar{u} = \bar{v} = 0$, for some long enough time. This results in a complex barotropic flow field that evolves with the wave which is used here as a background for TCs. As already mentioned, Ferguson et al. (2009) provides a detailed analysis of this flow for the case of a Kelvin wave. It is characterized by a wave-like phase-locked component that moves with the equatorial wave, superimposed on top

Table 1 Wave speed (c) of Kelvin, Rossby and MRG waves

Case	Wavenumber and gravity wave speed (m/s)	Kelvin	Rossby	MRG
1	$k = 1$ and $c_e = 1$	1	− 0.332	10.127
2	$k = 1$ and $c_e = 5$	5	− 1.637	24.142
3	$k = 1$ and $c_e = 15$	15	− 4.743	45.481
4	$k = 2$ and $c_e = 1$	1	− 0.329	5.333
5	$k = 2$ and $c_e = 5$	5	− 1.555	13.535
6	$k = 2$ and $c_e = 15$	15	− 4.110	27.571
7	$k = 4$ and $c_e = 1$	1	− 0.315	2.955
8	$k = 4$ and $c_e = 5$	5	− 1.293	8.427
9	$k = 4$ and $c_e = 15$	15	− 2.680	19.454
10	$k = 5$ and $c_e = 1$	1	− 0.306	2.487
11	$k = 5$ and $c_e = 5$	5	− 1.149	7.473
12	$k = 5$ and $c_e = 15$	15	− 2.125	18.069
13	$k = 8$ and $c_e = 1$	1	− 0.271	1.802
14	$k = 8$ and $c_e = 5$	5	− 0.774	6.170
15	$k = 8$ and $c_e = 15$	15	− 1.120	16.327
16	$k = 10$ and $c_e = 1$	1	− 0.245	1.584
17	$k = 10$ and $c_e = 5$	5	− 0.595	5.797
18	$k = 10$ and $c_e = 15$	15	− 0.780	15.873

of a spectrum of barotropic Rossby waves of various wavelengths. Similar flow patterns are obtained in the cases of ER and MRG waves (Hyun-Geun 2019).

We note that an initialization scheme for the TC is not needed because the equations of motion are solved with a stable numerical scheme that automatically dampens the grid scale noise and we have used an idealized synoptic vortex structure.

To illustrate, we plot in Figs. 2, 3, 4, the background barotropic flow induced by the Kelvin, Rossby, and MRG waves, respectively, at an arbitrary time T_0 and 12 h, 24 h, and 48 h later. The other wave parameters are as indicated in the Figure captions. Putting the wavenumber difference aside (which sets the size of vortices), we can see that in the case of the Rossby wave, irregular flow patterns, that nevertheless can carry disturbances near the equator westward, are generated while in the cases of Kelvin and an MRG waves, we have a superposition of sign alternating vortices on either side of the equator, leading to rapidly changing flow directions along the equator. Also noteworthy, the maximum wind speed induced by the Rossby wave forcing is an order of magnitude larger than it is in the other two cases.

Each forcing wave is characterized by a unique set of three parameters: the wave-type (Kelvin, ER, or MRG), a wavenumber, k, and an effective gravity wave speed, c_e. Table 1 reports all the equatorial wave parameter sets used in this study. The corresponding-actual wave speeds of the three equatorially trapped waves, depending on the wavenumber (k) and the effective gravity wave speed (c_e), are reported on the three last columns of Table 1.

At an arbitrary time T_0, during the simulation, the TC-like flow corresponding to (6) is injected into the simulation and allowed to freely interact with the wavefield-barotropic-flow background. This is repeated for T_0 values varying at 2 days interval, between 10 and 30 days yielding a total of 11 injection times for each set of equatorial wave parameters.

3 Results

3.1 First evidence of the equatorial wave effect on the TC trajectory

To briefly showcase the effect of equatorial waves on the TC trajectory, we report in Fig. 5 the TC trajectories by following the point of maximum vorticity (used here as a proxy for the TC centre) at every 6 h, in the longitude-latitude coordinates and for different wave conditions. The curve "ref" represents the reference TC trajectory corresponding to the case without a background flow.

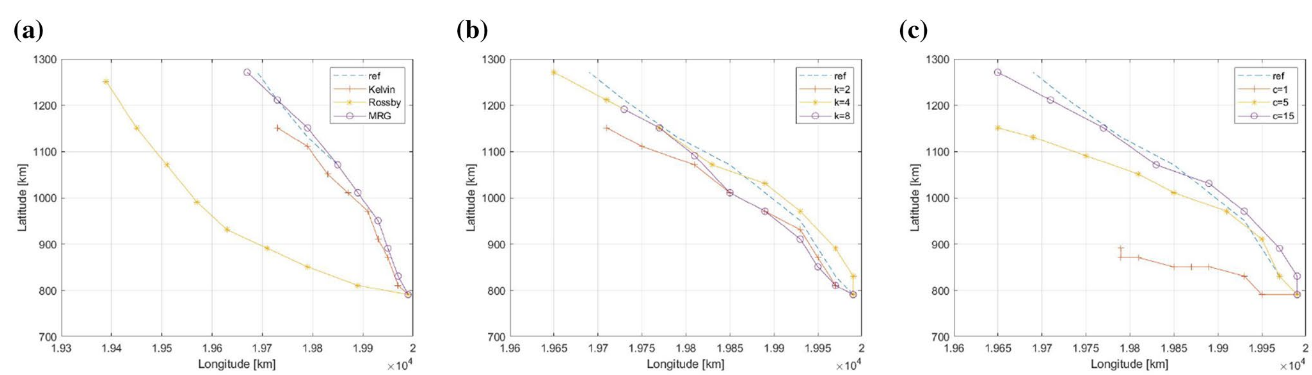

Fig. 5 TC trajectory change due to equatorial wave forcing with varying wave conditions. **a** Varying wave types: $k = 2, c_e = 15\text{m s}^{-1}, T_0 = 24$ days; **b** Varying wavenumber: Kelvin wave with $c = 15$ m s^{-1}, $T_0 = 22$ days and varying wavenumber; **c** varying phase speed: Kelvin wave with $k = 4, T_0 = 22$ days and varying phase speeds. See text for details

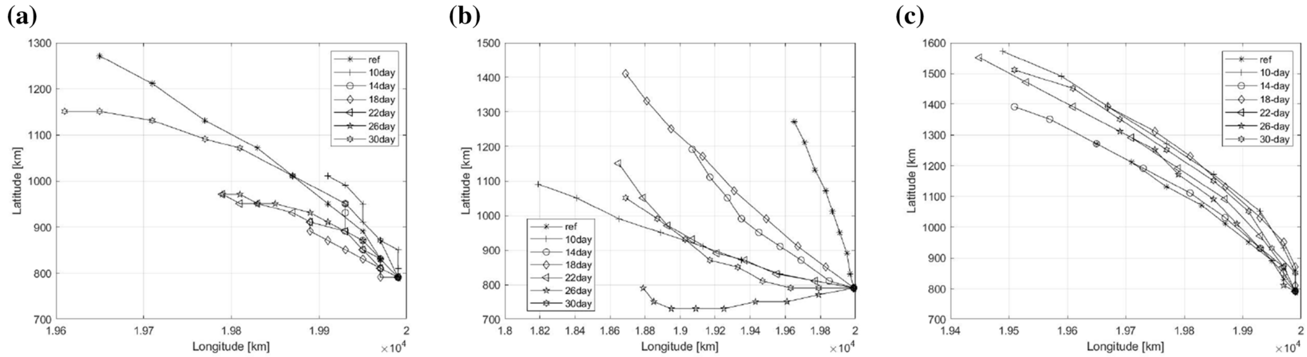

Fig. 6 TC trajectories in wave-induced background with different injection times, $T_0 = 10, 14, 18, 22, 26, 30$ days. The curve "ref" marks the reference TC trajectory corresponding to the zero background case. **a** Kelvin wave with $k = 5$ and $c = 1$ m/s. **b** Rossby wave with $k = 1$ and $c = -0.332$ m/s. **c** MRG wave with $k = 1, c = 1.802$ m/s

The plots in Fig. 5a represent the TC trajectories corresponding to the three equatorially trapped waves, Kelvin, Rossby, and eastward MRG of (n = 0 EIG) waves with the same wavenumber $k = 2$, the same equivalent gravity wave speed $c_e = 15$ m/s, and the same TC injection time $T_0 = 24$ days. The TC in the Rossby wave case has a completely different trajectory from the other two cases. For the first 24 h, it has lowest latitudinal locations, and then it changes direction and rapidly turns to the north. On the contrary, the trajectories in the other cases are very similar direction-wise. However, the TC in the Kelvin wave case has a shorter path compared to the reference while in the MRG case it is slightly longer. Our experiments suggest that TC trajectories in MRG wave-induced backgrounds typically remain close to the reference case unlike the case of Rossby and Kelvin waves. From the results in Fig. 5a, it is fair to conclude that the interaction of a TC with an equatorially trapped wave can significantly alter its trajectory and the effect may vary strongly depending on the wave type.

We now assess the dependence of this phenomenon on the other wave parameters. Figure 5b shows the TC trajectories for the Kelvin wave case using three different wavenumbers ($k = 2, 4, 8$) with the same phase speed $c = 15\,\mathrm{m\ s^{-1}}$ and the same TC injection time T_0 =22 days. As we can see, the traveling distance of the TC varies significantly depending on the wavenumber of the Kelvin wave forcing but the direction is relatively stable. The total travelled distance appears to be shorter than that of the reference case for wavenumbers $k = 2$ and $k = 8$ but larger for wavenumber $k = 4$. As we will see below, the TC traveling distance in a Kelvin wave background is typically shorter than that of the reference case and the overshooting in Fig. 5b associated with the case $k = 4$, is within the uncertainty due to the randomness in alignment of the TC with the phase of the wave associated with the TC injection time parameter T_0.

Figure 5c shows the TC trajectories in the Kelvin wave background for three wave speeds (c =1, 5, 15 m/s) but with the same wavenumber $k = 4$ m/s and the same injection time $T_0 = 22$ day. The TC appears to move at different angles, depending on the wave speed. The TC with c =1 m/s moves the shortest distance while the TC with c =15 m/s is very similar to the background-free reference case. These tests suggest that the Kelvin wave with lower wave speed restricts the movement of TC. This can be explained in part by the fact that the slower wave induces a phase locked barotropic response that moves at the same slow speed (Ferguson et al. 2009) and provides a longer residence time for the westward-northward moving TC. The slower moving Kelvin wave induced background seems to thus affect both the direction and the propagation speed of the TC.

3.2 Varying the TC injection time

As can be surmised from the numerical tests in Fig. 5, the tropical wave induced barotropic flow background has a non-trivial effect on the speed and direction of the TC drift and this effect is grandly influenced by the wave type, the wavenumber, and the phase speed. However, these tests are far from being conclusive in terms of determining which of this three parameters is the most influential or how each of these parameters affects the TC drift. Given that the wave induced background flow changes significantly in time and space (see Figs. 2, 3, 4), the phase of the wave at which this background enters into contact with the TC is of paramount importance; Independently on the flow strength, the effect of a cyclonic circulation on the TC trajectory is different from that of an anti-cyclone or a jet shear for that matter. The key parameter in our setting that controls the sensitivity of the TC movement to the wave phase at which the wave encounters the TC is in fact the injection time T_0.

In Fig. 6a–c, we report the TC trajectories in the wave induced background for different injection times, T_0, for the

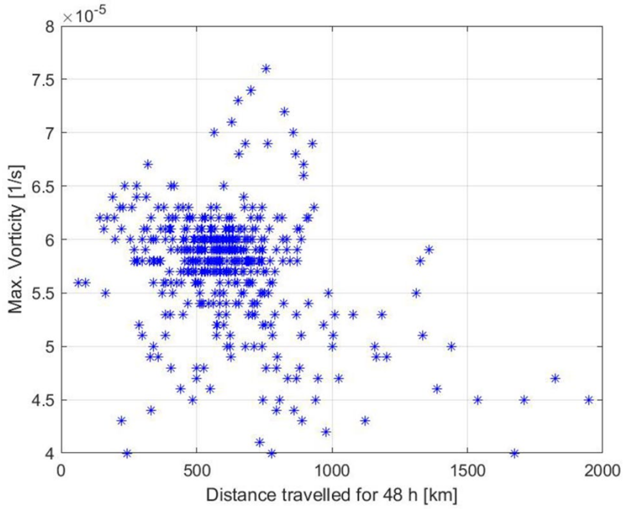

Fig. 7 Scatterplot of traveling distance and maximum vorticity at 48 h

case of the Kelvin, Rossby, and MRG waves, respectively. In each case the injection time, is varied from $T_0 = 10$ days to $T_0 = 30$ days. Four day increments are reported in Fig. 6 together with the reference trajectory corresponding to the case of a uniform-state-of-rest background. From the cases displayed in Fig. 6, we can see that the effect of the wave background on the TC depends strongly on the injection time T_0, i.e, on the phase of the wave at which the latter first encounters the TC. In other words the wave-TC alignment is critical to the TC trajectory. However, as can be seen from the three panels, the case of a Kelvin wave displays large variability in terms of the total distance travelled by the TC while there is a relatively smaller change in the propagation direction. This is consistent with the case of a varying wavenumber in Fig. 5b. For the Rossby wave case in Fig. 6b on the other hand, there is a large variability in both the distance travelled by the TC and its path direction. For the MRG case in panel (C), both the traveling distance and path direction are relatively stable.

A more comprehensive investigation of the sensitivity of the TC trajectory on the injection time is conducted and the results are reported in the appendix at the end of this article. The TC simulation is repeated for each one of parameter sets in Table 1 and for each TC injection time $T_0 = 10, 12, 14, \ldots, 30$ days. For each parameter set in Table 1, the statistics with respect to T_0 are considered and the corresponding mean path and standard deviation are computed and plotted in comparison to the uniform-zero background reference TC path. As expected, both the mean path and the associated variance change significantly with the wave parameters. Although, there is no clear pattern on how each one of the parameters influences the TC path in this statistical sense, a few conclusions can be drawn.

First, consistently to the results above, in the case of the Kelvin wave, apart from a few extreme cases that are deemed unrealistic, the direction of the mean path remains close to the reference path although the total traveled distance tends to be shorter while the associated variance is relatively small.

Second, in the case of the Rossby wave forcing on the other hand, the variance is very large in some cases, especially for the more physically relevant cases of small wavenumbers. The mean path appears to strongly depend on the phase speed. At $k = 1$ for example, for small Rossby phase speeds of $c = -0.332$ to -1.637 m s^{-1} the mean path direction is significantly to the west of the reference path while at $c = -4.637$ m s^{-1}, the mean path is significantly to the east of this reference. The associated variance also appears to increase with the phase speed at this wavenumber. At larger wavenumbers and larger wave speeds, we have both a small mean path deviation and a relatively small standard deviation. The total distance also appears to be more affected –longer–in the Rossby cases with small phase speeds and small wavelengths, that are more realistic, and it is much less so in the cases with higher wavenumbers and faster phase speeds.

Third, in the case of MRG waves, we found that the mean path direction is not very much affected, especially for the more physically relevant synoptic scale wavenumbers, $4 \leq k \leq 10$, and has a relatively small associated standard deviation, as in the case of the Kelvin wave, but the total distance traveled appears to be longer than the reference unlike the case of the Kevin wave.

3.3 A mechanistic analysis of the influence of the waves on TC trajectories

While it is clear from the results above that equatorially trapped waves have a non trivial effect on the trajectory of TC's through the generation of a non trivial barotropic flow background, a question of scientific interest is to determine the physical mechanism responsible for the this effect. There are two main mechanistic processes that determine the movement of a TC in a 2D barotropic flow: one is the beta-drift that allows the TC to propel itself by "riding" the ladder of the Coriolis force field and the other is through pure advection by the background wind. The key question is thus whether the tropical waves induce a change in the beta-drift mechanism or do they provide a background advection flow for the TC.

The change in the course of the TC trajectory through the beta-drift is possible only if the barotropic flow background induced by the tropical wave changes significantly the strength of the tropical cyclone by increasing or deceasing its vorticity maximum; Since the beta-drift is a result of the anti-symmetric flow induced by the

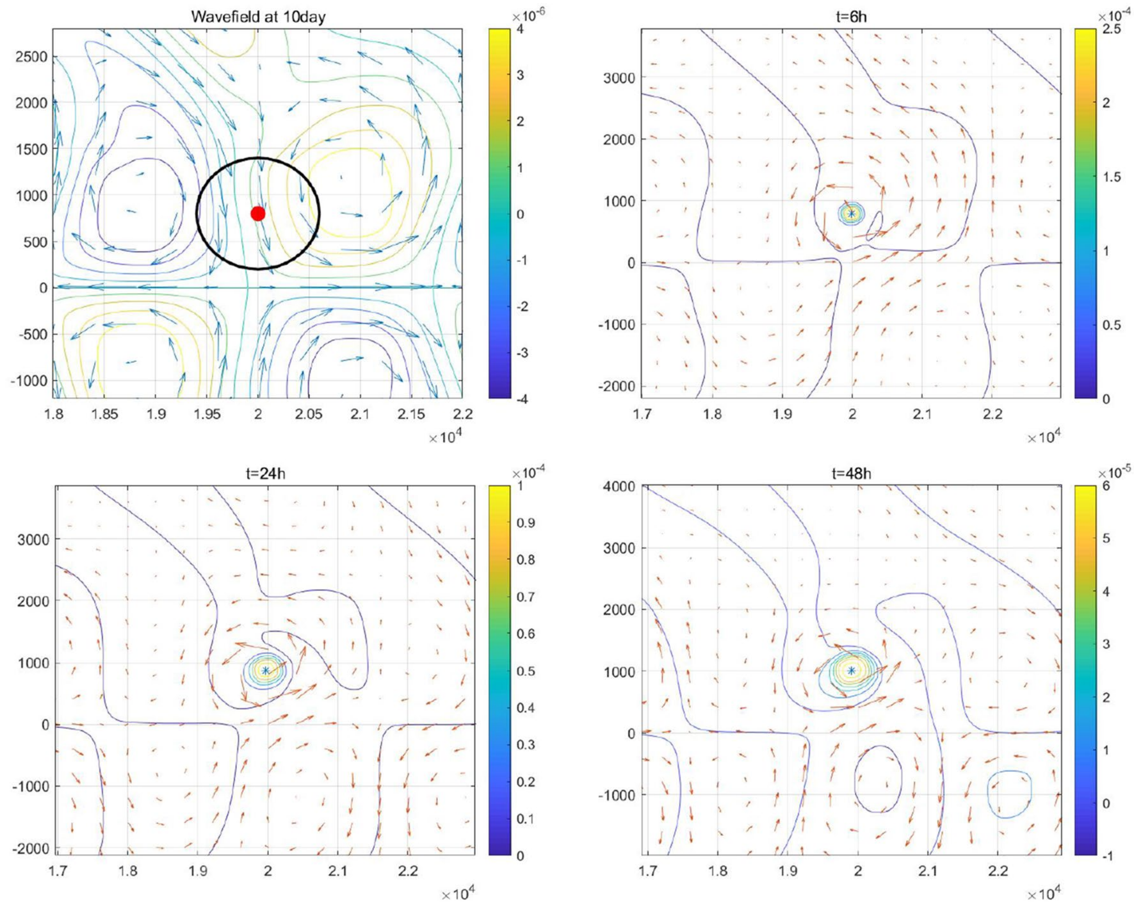

Fig. 8 Wave-induced background flow at the time of injecting the TC, in Kelvin wave case with $k = 5$, $c = 1$ m/s and $T_0 = 10$ days (top-left panel). The red dot in this panel marks the position of the TC when first injected into the simulation while the black circle marks the 5 m/s TC tangential velocity isoline. The other three panels show the total flow TC+background at later times. The arrows indicate the direction and strength of velocity field while the contours indicate the curves of constant vorticity. The largest arrow corresponds to a maximum speed of 2.00 m s^{-1} on the top-left panel (background flow alone), 16.04 m s^{-1} at 6 h, 10.88 m s^{-1} at 24 h, and 8.48 m s^{-1} at 48 h

interaction of the vortex and the Coriolis-gradient field, the TC propagation speed is an increasing function of the TC vorticity maximum.

Thus, to address whether the change in TC trajectory induced by a change in the vorticity maximum, here, we examine the relation between the change in the 2 day-travelling distance of the TC centre, due to the presence of the tropical waves, and the change in the TC maximum vorticity. A scatterplot of the maximum vorticity, evaluated at 48 h after the TC is injected into the wave background, and the Euclidean distance, $||P_{48h} - P_0||$, travelled by the TCs in 48 h is shown in Fig. 7. Here P_t is the position of the TC centre at time t and $||.||$ is the Euclidean distance. Each data point in Fig. 7 corresponds to one experiment with the parameters in Table 1 and T_0 varying from 10 to 30 days at 2 day intervals ($18 \times 11 = 198$ experiments in total). While it is clear that the wave background induces a significant change in the TC vorticity maximum, which varies between 4×10^{-5} s^{-1} and 8×10^{-5} s^{-1}, the distribution of the data points in Fig. 7 does not suggest a relationship between the change in vorticity maximum and the change in the 48 hour traveling distance.

To push the analysis a bit further, we compute the correlation coefficient between the two quantities, given by

$$C_{\xi,d} = \frac{\sum_{j=1}^{n} \Delta\xi_j \cdot \Delta d_j}{(\sum_{j=1}^{n} \Delta\xi_j^2)^{1/2} (\sum_{j=1}^{n} \Delta d_j^2)^{1/2}}. \tag{7}$$

Here, d_j is the straight distance for case j, d_{ref} is the straight distance of the reference and $\Delta d = d_j - d_{ref}$. ξ_j is the maximum vorticity of case j, ξ_{ref} is the reference maximum vorticity, corresponding to the wave-less background case, and $\Delta\xi_j = \xi_j - \xi_{ref}$.

The calculated $C_{\xi,d}$ is about -0.3585, which means that the two quantities are only weakly correlated and in fact, negatively correlated, contrary to the known fact that the TC propagation speed due to beta-drift increases with the maximum vorticity. It is thus fair to suggest that the change

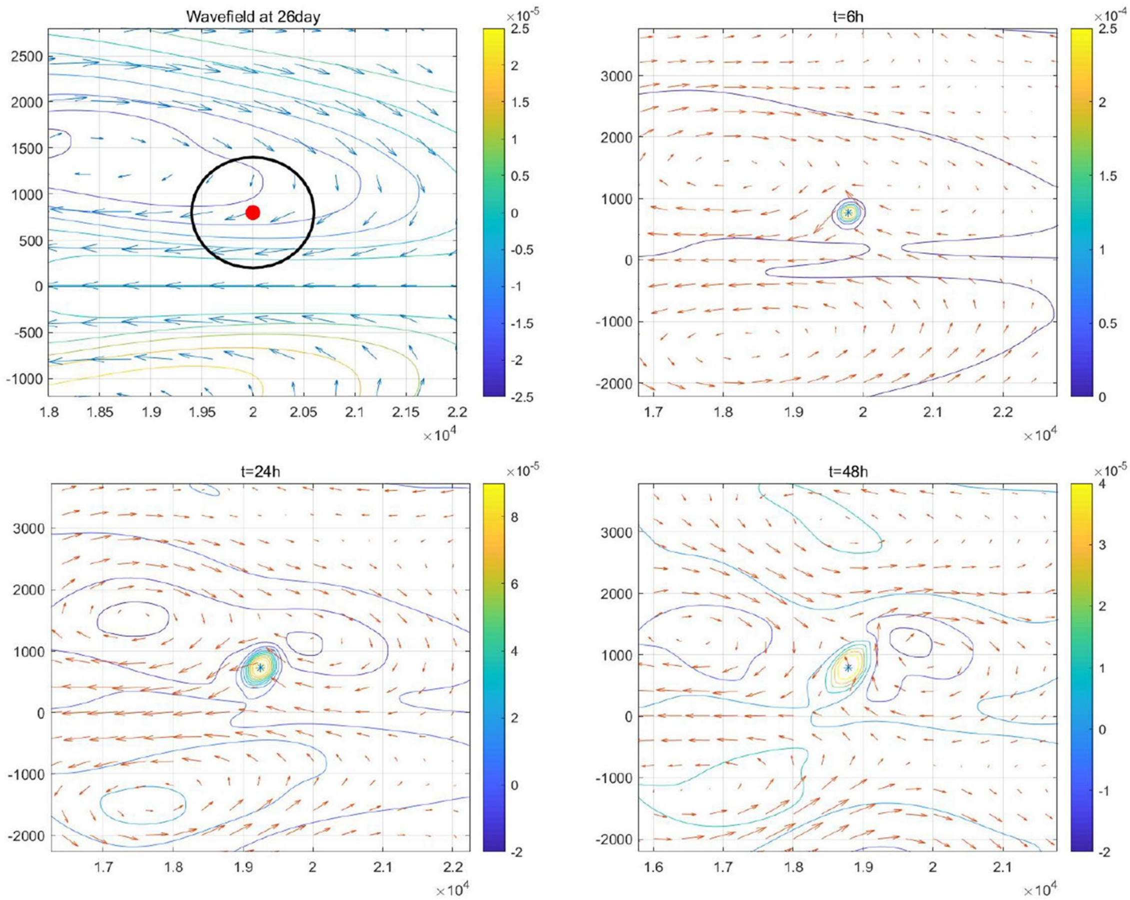

Fig. 9 Same at in Fig. 8 but the case of the Rossby wave with $k = 1$, $c = -0.332$ m/s and $T_0 = 26$ days. The largest arrow corresponds to a maximum speed of 14.5 m s^{-1} on the top-left panel (background flow alone), 21.10 m s^{-1} at 6 h, 13.80 m s^{-1} at 24 h, and 9.22 m s^{-1} at 48 h

of vorticity maximum of the TC is not the main or direct cause of the change in TC trajectory due to the presence the equatorially trapped waves. Therefore, the advection by the background flow, induced by the waves, is assumed to be the primary driver for the change in the TC trajectory.

As can be surmised from the pictures in Figs. 2, 3, 4, the wave-induced background-advection flow is indeed very complex, time dependent and depends heavily on both the wave parameters (wave type, wavenumber and wave speed) and the phase of the wave at which the TC is injected. For this reason, a thorough analysis on how the waves precisely stir the TC depends on all these factors and it is beyond the scope of the present study. Instead, we illustrate this by two examples, one corresponding to the Kelvin wave forcing and the other corresponding to the case of a Rossby wave forcing in Figs. 2 and 3, respectively. While the illustrations are far from being conclusive, the hope is that they'd provide some background intuition consistent with the idea that the change in the TC trajectory is due to the advection of the vortex by the induced background flow.

Figure 8 illustrates the moving TC as it interacts with the Kelvin wave background for the case $c = 1$ m s^{-1} and $k = 5$. The background flow at the time at which the TC is injected is shown on the top-left panel. We note that four opposing vortices located on either side of the equator are captured in this panorama. It is important to note however that the same flow pattern extends in both directions (north-south and east-west) as an array of vortices that do not diminish in strength away from the equator unlike the mother wave that created them (Ferguson et al. 2009; Hyun-Geun 2019). The red dot is the centre of the TC, and the black circle around it indicate the level curve where the TC tangential velocity is 5 m/s to indicate the TC size relative to the background flow. Initially, the TC is located on a strong and narrow wind channel directed to the South-towards the equator. This situation lasts for the whole TC simulation period of 2 days because of the slow wave speed and the large scale of the wave. The development of a negative vortex beside the TC may not be of any influence, but the northward movement of the TC is prevented by the background wind. The other three panels show the total flow field of the evolving TC

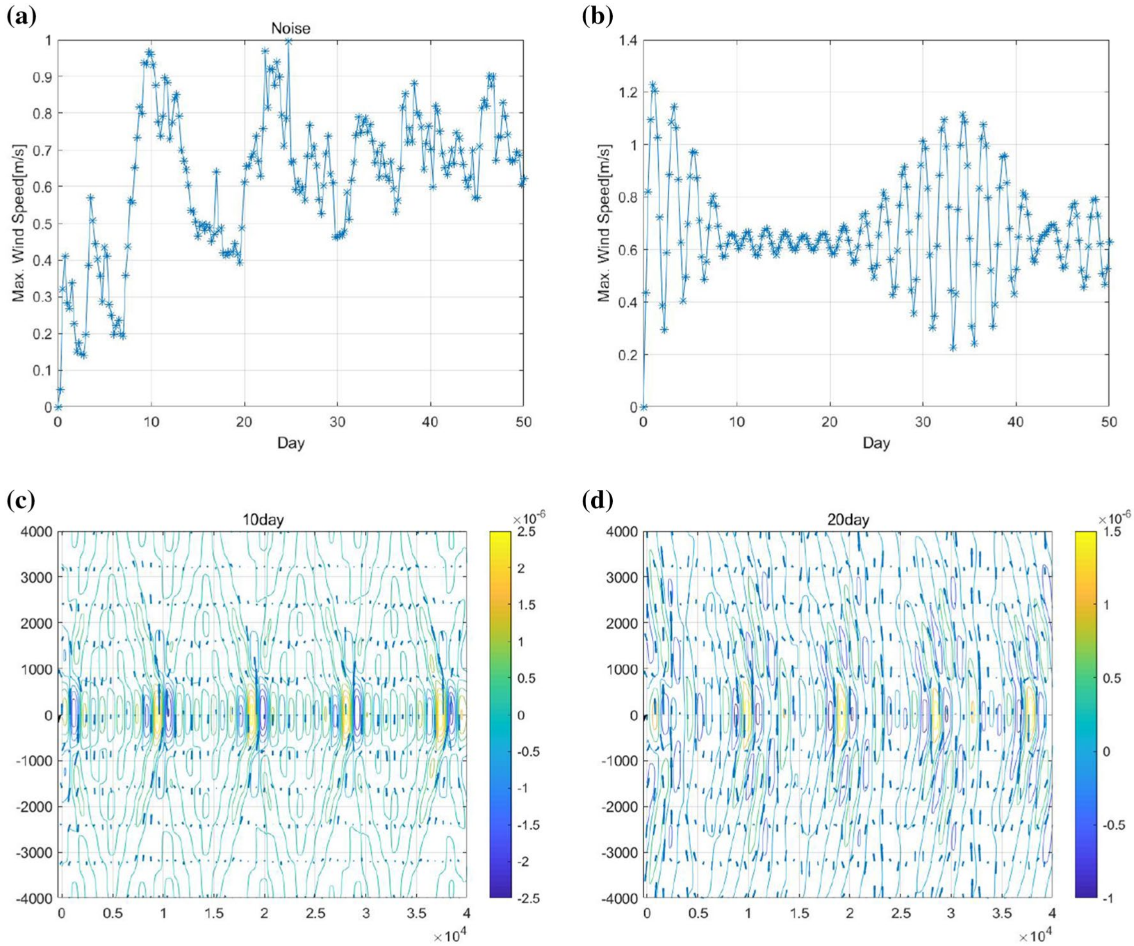

Fig. 10 **a** Time series of maximum wind speed for the barotropic flow generated by the correlated stochastic noise in (8). See text for parameter values. **b** Same as **a** but when the Kelvin wave forcing, with $k = 5, c = 15$ m/s and $A = 15$ m/s, is used. **c**, **d** Snapshots of the bartropic vorticity filed (1/s) generated by the stochastic noise forcing in (8) at 10 days and 20 days, respectively

which is superimposed on the wave-induced background wind field. For this particular case, the TC centre had hardly moved. This is indeed expected since the TC finds itself trapped between two vortices (a cyclone to the East and an anti-cyclone to the West) that are exactly opposite to the beta-induced anti-symmetric gyres that lead to a North-West movement of the TC and the latter finds itself trapped near the equator. While this clearly an extreme case, it showcases how in the case of a Kelvin wave the TC traveling distance can be reduced. It has to be noted that circumstances where the TC can land in a completely opposite phase that would accelerate its Northwest movement is also possible but in that case the TC will quickly exit that environment and end up in a hostile situation similar to the one illustrated here (see Fig. 2).

In Fig. 9, the TC is injected in a flow background induced by a Rossby wave with $k = 1$ and $c = -0.332$, at $T_0 = 26$ days (see also Fig. 3). Here, the TC finds itself in the middle of a big negative vortex and gets affected by a strong wind directed westward. At 6 h, there are two arrows inside the TC. One is much stronger and points northwestward while the weaker one points in the southwest direction. Besides, there is a wind field running counterclockwise to the West of the TC, which prevents the TC from moving to the North. As time goes by, the surrounding flow becomes stronger, c.f. the flow field at 24 h. Thus, it takes a longer time for the TC to develop enough negative vorticity to its right side in order to move Northward while the TC moves to the West continuously. The lopsided shape of the TC delineates how strong the wind field pushes the TC. Furthermore, there is a big negative vortex just above the TC at 24 h. While the vortex is prevented from moving Northward it finds itself accelerated toward the West, which allows it to travel overall a longer distance in 48 h.

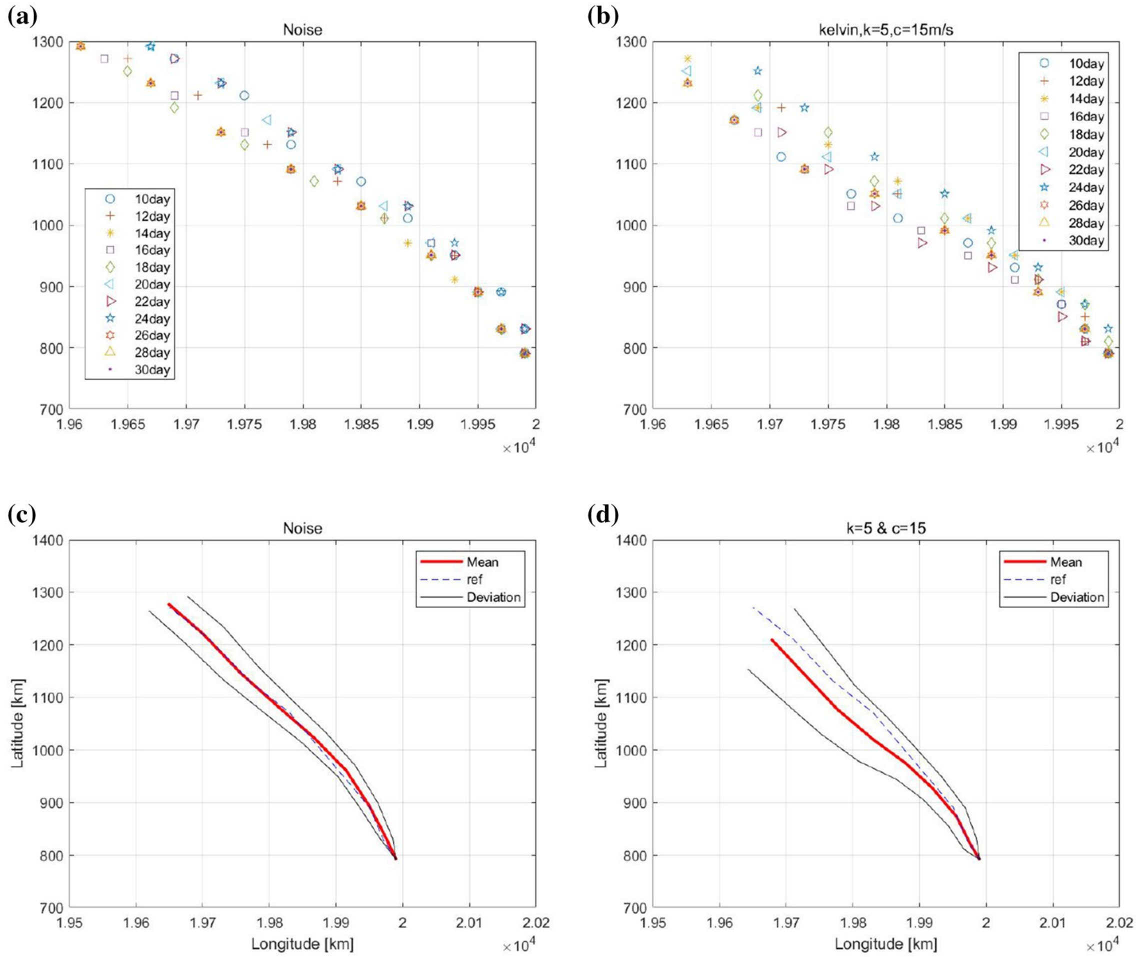

Fig. 11 2 day TC paths of all the cases corresponding to TC injection times $T_0 = 11, 13, 15, 30$ days for the case of random forcing (**a**) and a Kelvin wave forcing (**b**). **c**, **d** and the mean path (red) of deviation (black) curves corresponding to the random forcing and Kelvin wave forcing, respectively. The dotted lines on each panel correspond to the reference path of the TC evolving in a homogeneous flow-less background

3.4 Robustness test using a stochastic noise forcing

To demonstrate the robustness of the results presented in the previous subsections, suggesting that the equatorial waves have a distinctive influence on the TC movement, an it is not all just a matter of randomness, here we consider the vorticity equation in (2) when the forcing on the right hand side is replaced by a correlated stochastic noise on the form (Berner et al. 2009)

$$F = \frac{\hat{\beta}}{\triangle t} \sum_{k=1}^{5} \sum_{l=-k}^{k} (k^2 + l^2)\phi(t) \sin[2\pi(kx/L_x + ly/L_y)], \quad (8)$$

where the noise amplitude $\phi(t)$ is a Markovian-type stochastic process,

$$\phi(t + \triangle t) = (1 - \alpha)\phi(t) + g_k \sqrt{\alpha}\epsilon(t), \qquad g_k = bk^p.$$

Here, $\epsilon(t)$ is a standard Gaussian random variable while $\alpha = 0.4, b = 1, p = -1.27$ are fixed constants. The quantities L_x, L_y are the computational domain extents in the x and y directions, respectively, and $\triangle t$ is the model time step. The coefficient $\hat{\beta} = 0.5 \times 10^{-5}$ is a non-dimensional parameter that fixes the overall scale of the forcing. This type of correlated noise is used in long-term weather prediction models to represent the energy backscatter from unresolved wave turbulence (Berner et al. 2009). The parameter values are carefully chosen so that the barotropic response flow is comparable to the ones generated by the tropical waves above both in terms of magnitude and length and time scales.

Equation 8 uses a combination of five different wavelengths in both x and y, ranging from synoptic to planetary scales that mimic the range of scales used in the equatorially trapped wave tests used in the previous section. Combined with the Markovian-type Gaussian noise amplitude, it forms a noise forcing which is correlated in both time and space. We note also that the time scale of the noise variability is controlled by the parameter g_k which is set to depend on the zonal wavenumber k and the coefficient b that are specifically chosen to yield variability time scales that are comparable to those induced by the equatorial wave forcing. This is corroborated by the resulting barotropic response maximum-wind timeseries plotted in Fig. 10a, when compared to Fig. 10b that that corresponds to the case of our typical Kelvin wave forcing.

Two time snapshots of the barotropic vorticity, generated by the random forcing in (8), are shown in Fig. 10c, d. They correspond to the simulation times 10 days and 20 days, respectively. While the randomly generated vorticity has a comparable magnitude as that generated by the equatorial waves in Figs. 2, 3, 4, its overall structure is significantly different. For instance, in all the tropical wave cases, in Figs. 2, 3, 4, the vorticity maximum and minimum are attained off the equator while in the random forcing case, the vorticity maximum and minimum are found along the equator. Also, while the individual wave forcings offer distinctive wavelength of the most energetic gyres that corresponds to half of that of the parent wave (Ferguson et al. 2009), the random forcing seems to have a more uniform scale character.

As in the previous experiments, the simulation with the random noise is repeated multiple times and the TC-like flow in (6) is injected into the simulated flow at time $T_0 = 11, 13, \ldots, 28, 30$ days, and the TC-bearing simulation is carried during two more days. The 2 day-long paths of the TC are plotted in Fig. 11a for each one of the simulations corresponding to the injection times $T_0 = 11, 13, \ldots, 28, 30$ days. The Kelvin wave forcing analogues are (re)plotted in Figure 11b for comparison. The resulting mean and deviation paths are reported in Fig. 11c, d, respectively. As we can see, as expected from the differences in the generated vorticity fields in Fig. 10c, d, the TC paths corresponding do the random noise forcing and that of the tropical wave have important differences. For instance, compared to the reference mean path (dashed curves), for TC's evolving in a randomly generated background flow, the mean path is unchanged and the deviation is relatively contained but in the case of the Kelvin wave generated background flow, the mean TC path is both shorter and is pushed to the left (east) by a few hundred kilometres as already pointed out.

These results corroborate our previous results which suggest that tropical waves have a distinctive effect of the path of tropical cyclones, that the mere stochastic forcing cannot possibly emulate as this effect may depend on various factors such as the wavelength, the wave phase speed, or the wave-type.

4 Conclusions

The observed movement of tropical cyclones (TC) in the northwest direction in the northern hemisphere and southwest direction in the southwest hemisphere is known to be induced by the interaction of the TC with the Coriolis force gradient, a phenomenon simply called the beta drift or beta effect (Fiorino et al. 1989; Li and Wang 1994). The beta effect leads to the formation of an asymmetric flow consisting mainly of two vortices of opposite sign distributed on two opposite sides of the TC in such a way that they induce a flow field that propels the TC in, accordingly, the north- or southwest direction (Fiorino et al. 1989; Wang and Li 1992; Chan and Williams 1987). However, it is also well known that the presence of a background flow such as a monsoon trough or a synoptic scale jet shear can alter the path of the TC quite significantly (Williams and Chan 1994).

It has been hypothesized that TCs are generated near the equator from the amplification of pre-existing vortices that are sometimes directly or indirectely linked to equatorially trapped waves (Carl and Schreck 2012; Kiladis et al. 2009). Since these waves contribute to the formation of TCs, it is naturally suggestive that they can affect their movement from the beginning of their formation. Here, the effect of equatorially trapped waves on the TC trajectory is numerically studied based on a barotropic model in an equatorial beta-plane approximation. To illustrate this, we consider Kelvin, Rossby and eastward MRG waves with various wavenumbers and wave speeds. Although, it intuitively constitutes an important parameter on which this effect strongly depends, the wave amplitude is fixed to the moderate value of 15 m s^{-1} and we focussed instead on the variations in wavenumber and wavespeed because the expected dependence may be very subtle. The waves provide a baroclinic forcing which induces a barotropic response that depends on these wave parameters. A TC is injected into the wavefield-background at some arbitrary time T_0 during the simulation and the cyclone trajectory is monitored during the following 2 days.

It is found here that the change in the TC trajectory due to the presence of wave-induced background depends widely on the wave parameters, including the wave types (here Kelvin, Rossby or MRG), the wavenumber, and the phase speed, as well as the TC injection time T_0, which can be regarded as the phase of the wave at which the wave encounters the TC. Three groups of wavenumbers, k, and three groups of phase speeds, c, parameters were considered. Wavenumbers $k = 1, 2$ represent planetary scale waves, wavenumbers $k = 4, 5$ represent long-synoptic scale waves and $k = 7, 8$ are meant to represent short-synoptic scale waves. Similarly, the phase speed parameter is varied from very slow, to slow, to

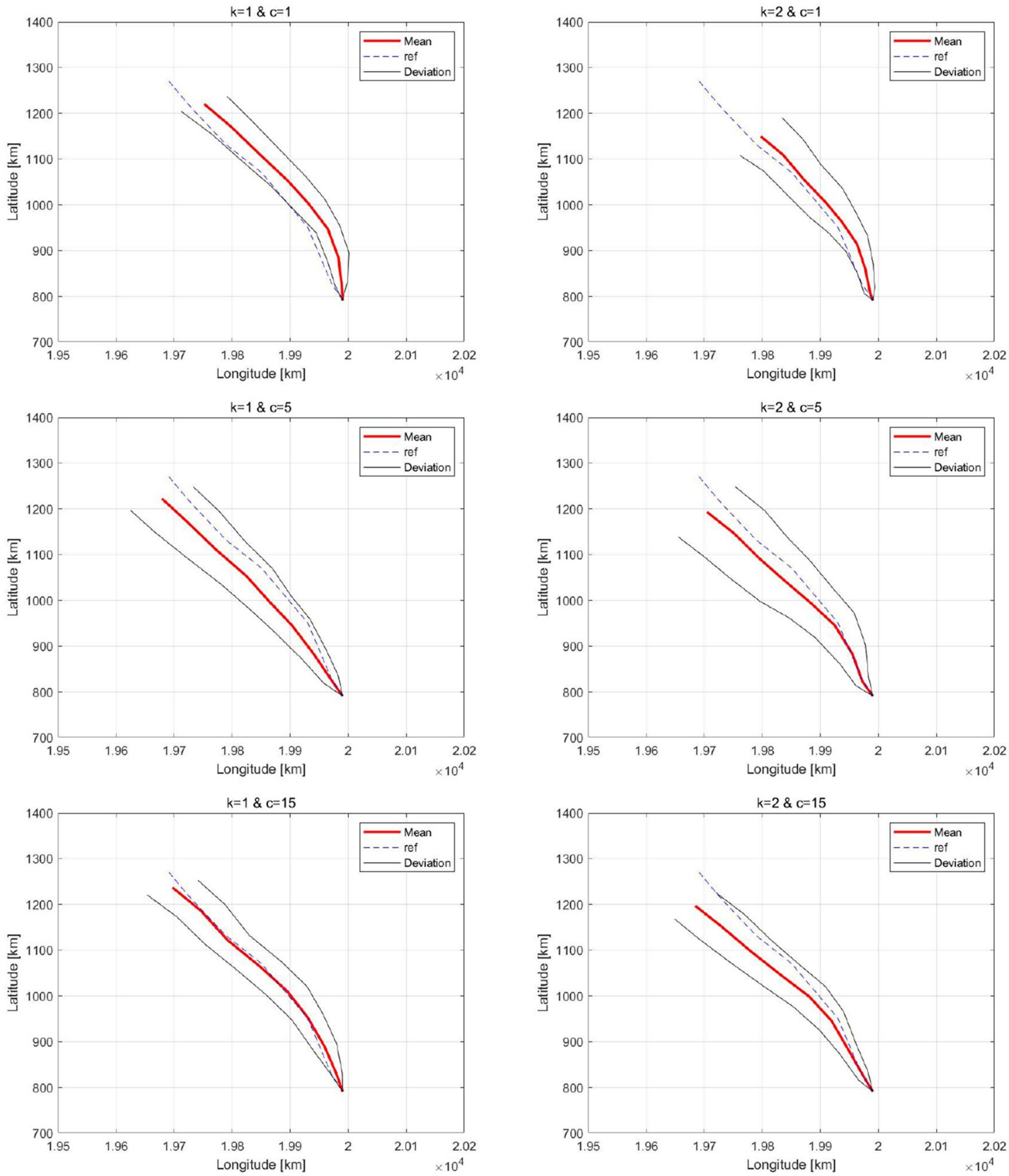

Fig. 12 Mean path and its deviations of TC trajectories in Kelvin wave with (from left to right, top to bottom) $k = 1, c = 1$ m/s, $k = 2, c = 1$ m/s, $k = 1, c = 5$ m/s, $k = 2, c = 5$ m/s, $k = 1, c = 15$ m/s, $k = 2, c = 15$ m/s. In each cases The statistics were taking for TC varying injection times $T_0 = 10, 12, 14, \dots, 30$ days

moderate, corresponding to the equivalent gravity speeds $c_e = 1\ \mathrm{m\ s^{-1}}$, $c_e = 5\ \mathrm{m\ s^{-1}}$, and $c_e = 15\ \mathrm{m\ s^{-1}}$, respectively. We note that $c_e = 15\ \mathrm{m\ s^{-1}}$ corresponds to the observed speed of convectively coupled Kelvin waves and $c_e = 5\,\mathrm{m\ s^{-1}}$ is the propagation speed of the Madden-Julian oscillation (Kiladis et al. 2009) while the speed $c_e = 1\mathrm{m\ s^{-1}}$ is arguably unrealistic and used here as a sensitivity-benchmark parameter value.

Both the direction and the average speed (as inferred from the distance travelled by the TC in 48 h) of propagation vary significantly with these parameters. However, in the realistic parameter regimes of synoptic scale moving at $15\ \mathrm{m\ s^{-1}}$ as observed in nature, Kelvin waves are found to make TCs travel a shorter distance without altering too much the direction of propagation. It is also the case when the Kelvin wave speed is $5\ \mathrm{m\ s^{-1}}$ and has a planetary scale wavelength which

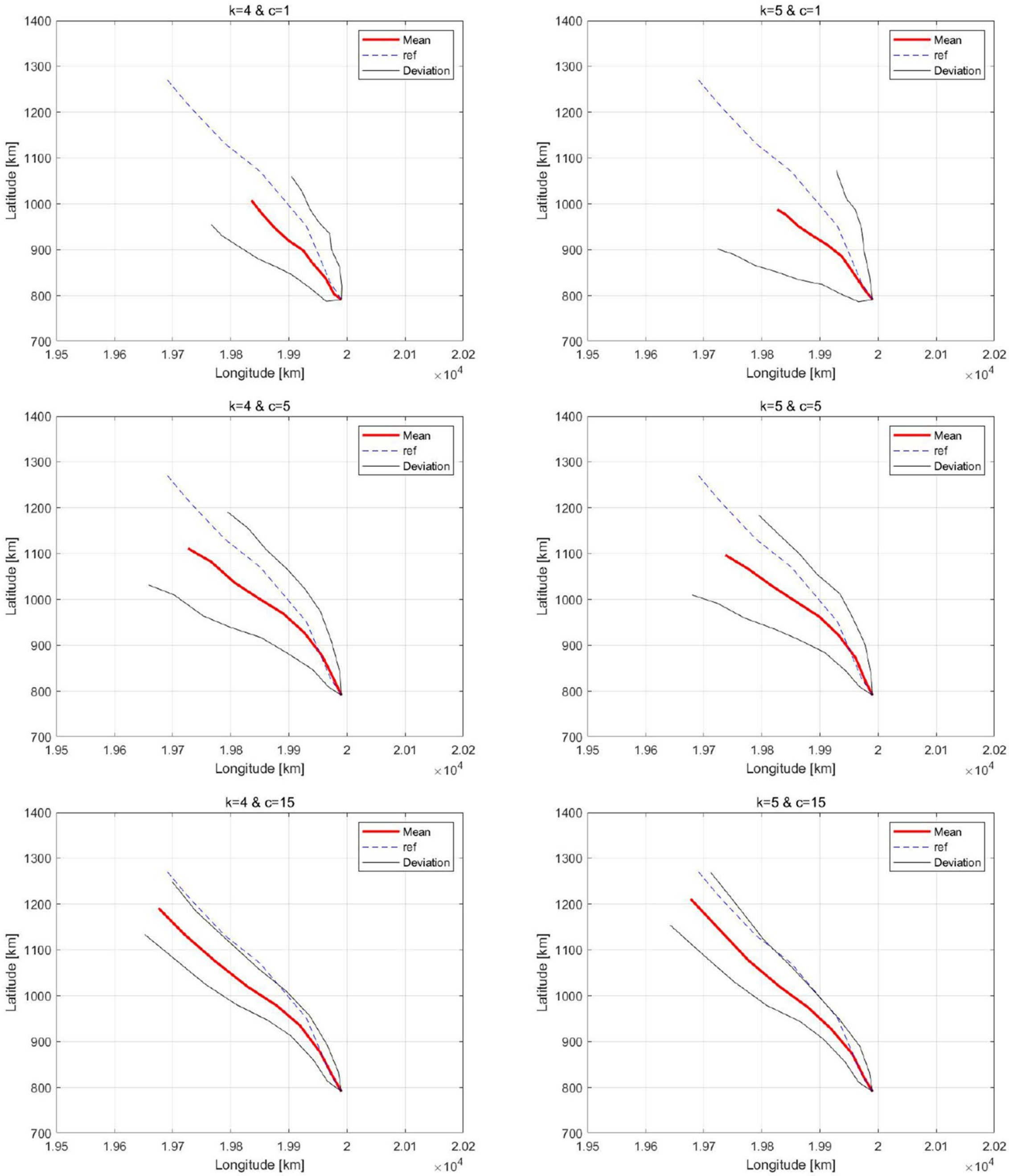

Fig. 13 Same as Fig. 12 but for k =4, 5

maybe related to the MJO. However, a thorough study of this effect by a more realistic MJO model is necessary before we can draw a definitive conclusion. One possibility will be to use the MJO-skeleton of Majda and Stechmann (2009) to force to the barotropic model. TCs in Rossby and eastward MRG wave backgrounds on the other hand seem to move longer distances. However the MRG impact is relatively less significant in many wave parameter regimes. More importantly, TC trajectories in Rossby wave backgrounds have a wide range of trajectories both in terms of direction and in terms of speed and depend strongly on the injection time, i.e, the wave phase.

To test the robustness of these results, we also considered the case where the background flow is generated by a random noise forcing that consists of a time and space correlated noise that mimics the energy backscatter from unresolved wave turbulence in weather prediction models (Berner et al. 2009). It is found that on average the random

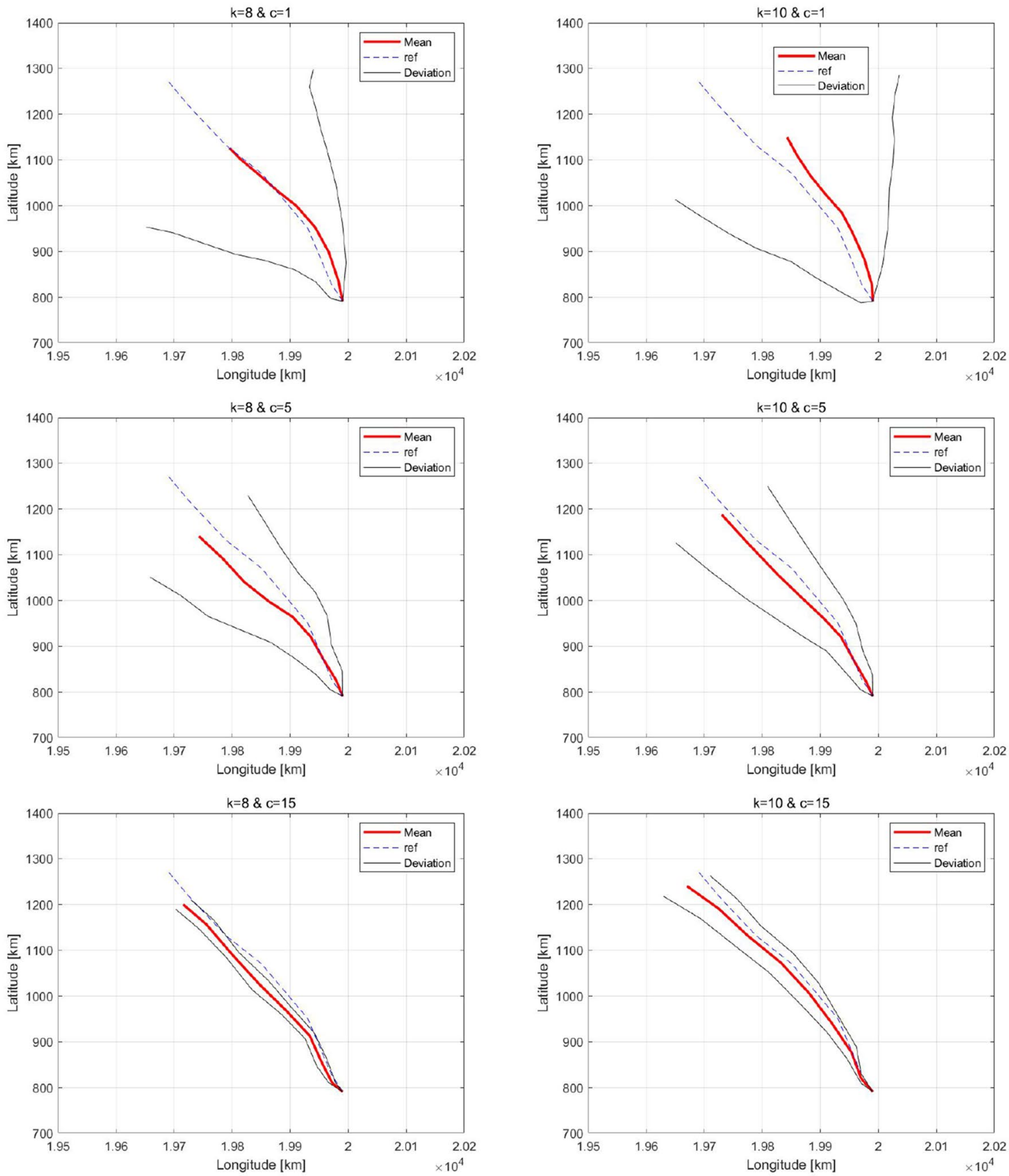

Fig. 14 Same as Fig. 12 but for k =8, 10

noise has no effect on the TC path and that the deviation is less than the typical Kelvin wave case for example. It is thus reasonable to suggest that tropical waves have a distinctive effect of the path of tropical cyclones that the mere stochastic forcing cannot possibly emulate.

There are two different mechanisms through which equatorial waves can change the course of a TC trajectory: (1) the equatorial wave can exchange kinetic energy with the TC and make it stronger or weaker in such a way to interfere with the beta-gyres or that (2) the induced wave-field simply transports the TC vorticity by pure advection as in the case of a classical large-scale flow background (Williams and Chan 1994). To elucidate this issue, we produced the scatterplot of the change in TC traveling distance and the change is the TC's maximum vorticity, induced by the presence of the equatorial wavefield-background. Our analysis shows that

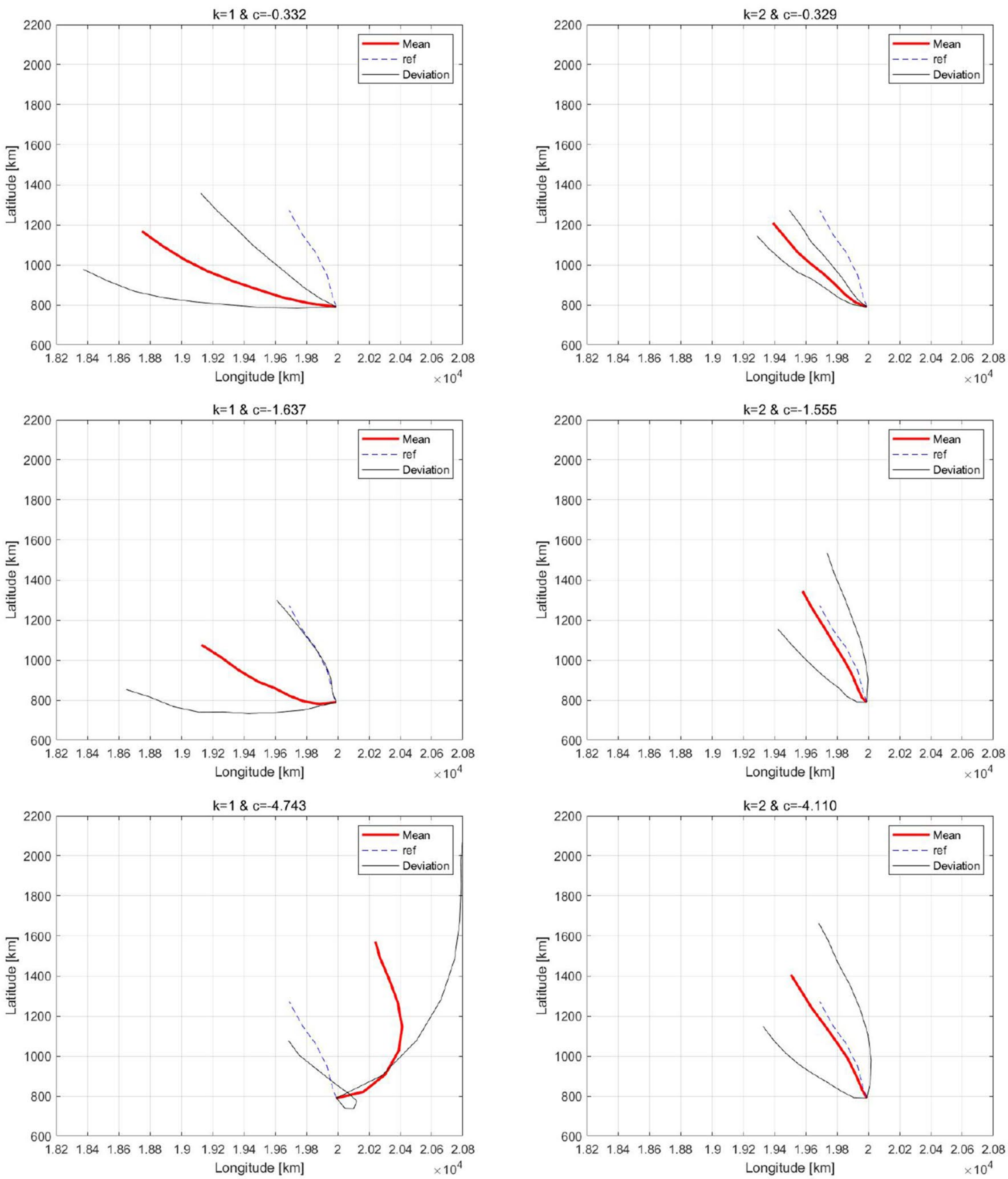

Fig. 15 Same as Fig. 12 but for the Rossby wave

the two quantities are only slightly negatively correlated. This suggests that the effect of equatorially trapped waves on the TC trajectory is primarily due to pure vorticity advection while kinetic energy exchange between the TC and the wave which is undeniably present has very little to no effect on the TC trajectory. This point of view is consistent with the blowup illustrations in Figs. 8 and 9 that showcase the background flows in respectively two typical Kelvin and Rossby examples.

Appendix: Mean TC path and standard deviations for various tropical wave forcings

To undertake a more comprehensive investigation of the effect of the wave-induced background of the TC trajectory, we consider each one of the cases in Table 1 and vary the TC injection time T_0 from $T_0 = 10$ days to $T_0 = 30$ days with a uniform 2 day increment, yielding a total of 11 samples for each case. In Figs. 12 through 20, we report the mean path

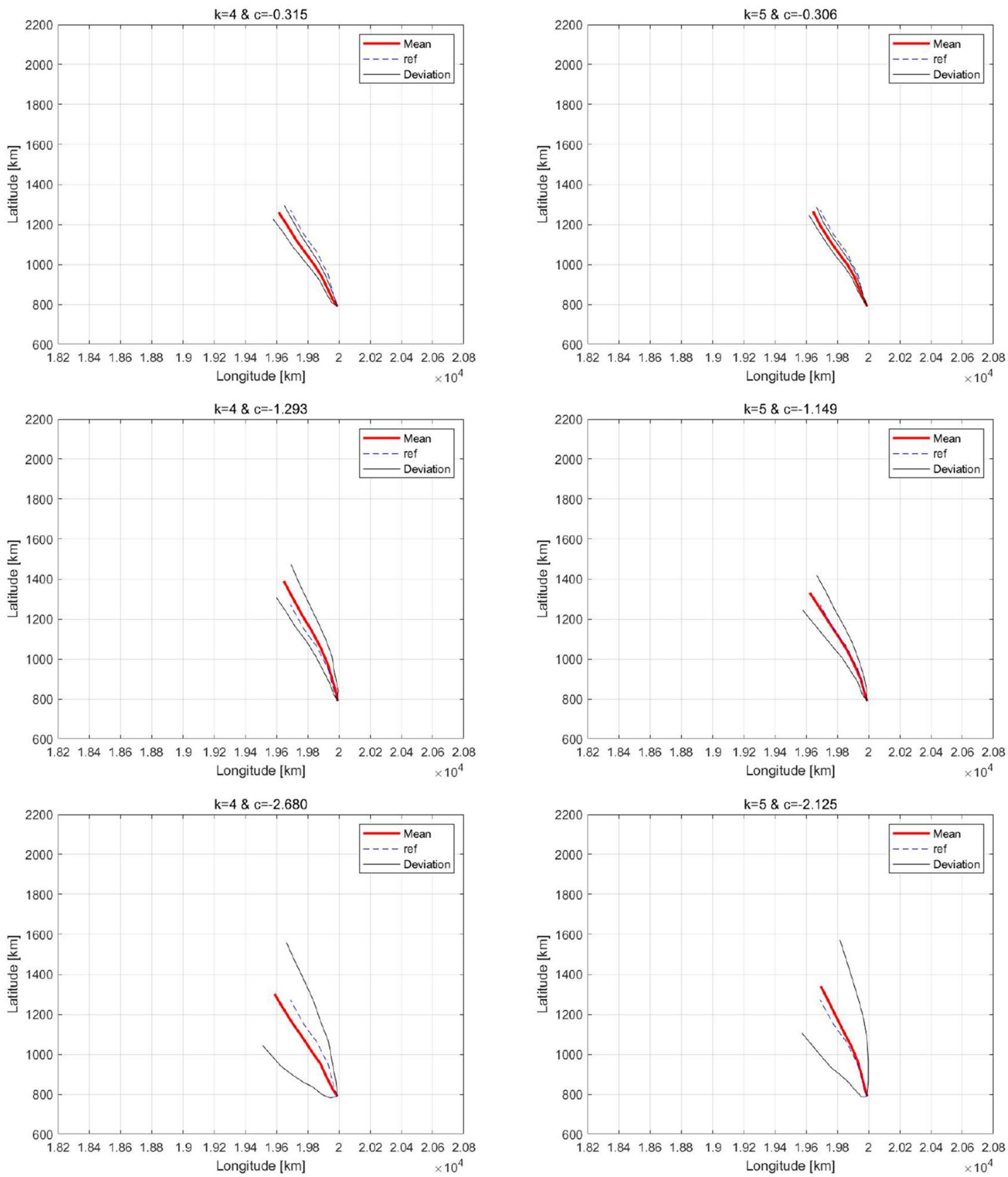

Fig. 16 Same as Fig. 15 but for $k = 4, 5$

and the cone of trajectories represented by the mean path plus and minus one standard deviation, when T_0 is varied as just described, for each one of the test cases in Table 1. In all these panels, the blue-dashed curve labeled "ref" represents the zero-background reference trajectory, the red curve represents the statistical mean path and the thin black curves are the standard deviations. A fixed reference scale is used on all panels of each wave type to ease the comparison.

For each wave type, we consider six wavenumbers, grouped into three categories: planetary scale ($k = 1, 2$), upper synoptic scales ($k = 4, 5$), and lower synoptic scales ($k = 8, 10$), and three wave speeds, also representing three categories: very slow corresponding to a gravity wave speed $c_e = 1$ m s^{-1}, slow corresponding to a gravity wave speed $c_e = 5$ m s^{-1} and moderate corresponding to $c_e = 15$ m s^{-1}. We note that in the case of the Kelvin wave, the actual phase

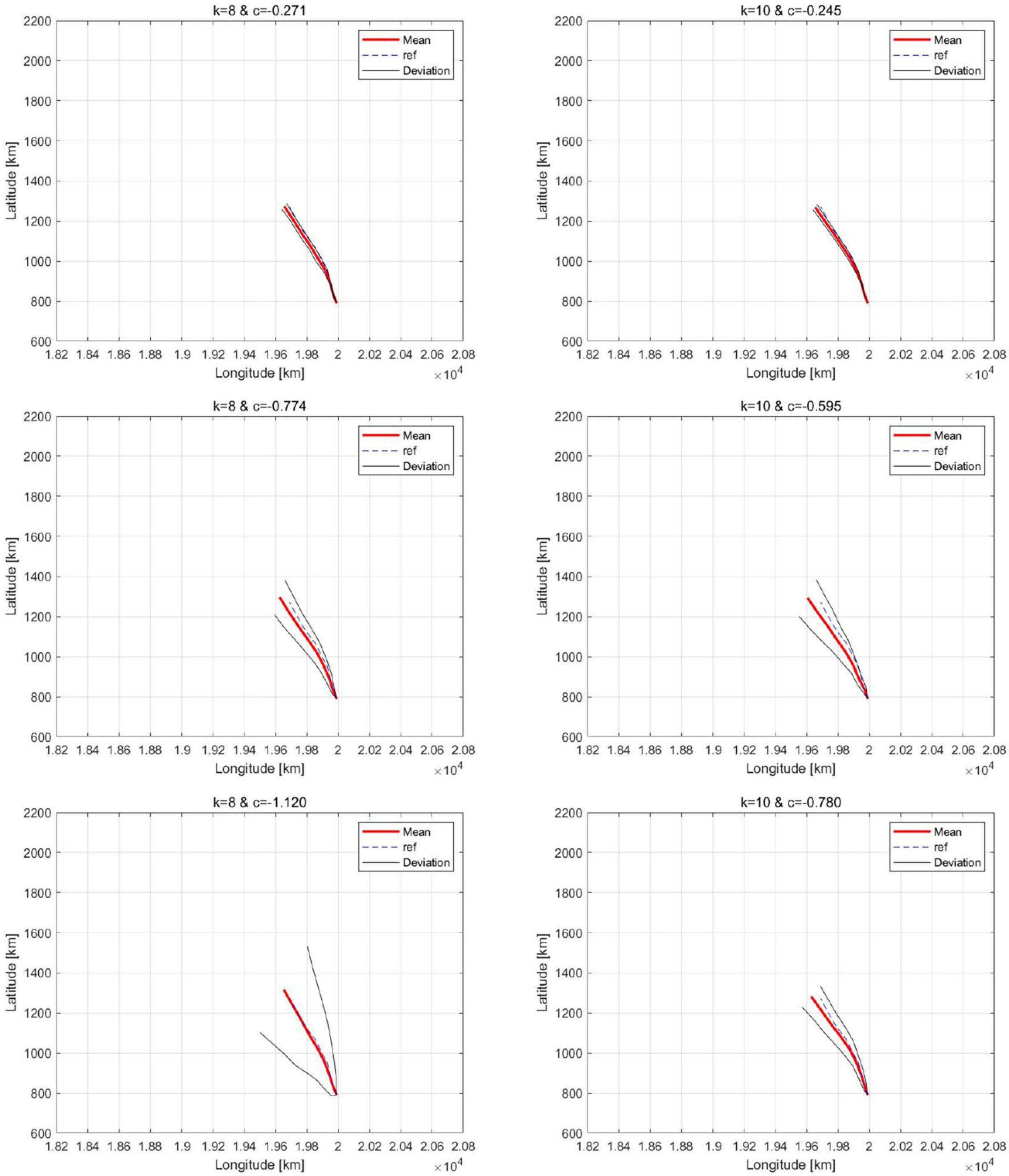

Fig. 17 Same as Fig. 15 but for $k = k = 8, 10$

speed is the same as the imposed gravity wave speed ($c = c_e$) while in the other two cases the phase speed depends on both the gravity wave speed and the wavenumber. See Table 1.

From the plots in Figs. 12 through 20, we can see that both the mean path and the associated variance depend on the above wave parameters. Although there is no clear pattern, we can see that in the case of a Kelvin wave background that, apart from a few exceptions, the mean path remains fairly close to the reference path, especially in terms of the direction of propagation and that the variance is relatively small. In all cases, the average total distance travelled (as measured by the arc length of the mean path) is consistently smaller than its reference counterpart. The few exceptions are associated with the cases of slow phase speeds and synoptic scale wavenumbers, corresponding to $c = 1, 5\,\mathrm{m\ s^{-1}}$ and $k = 4, 5, 8, 10$ in Figs. 13 and 14 and display a remarkably smaller mean path distance and much larger variance. In retrospect, such cases are hardly realistic as Kelvin waves are

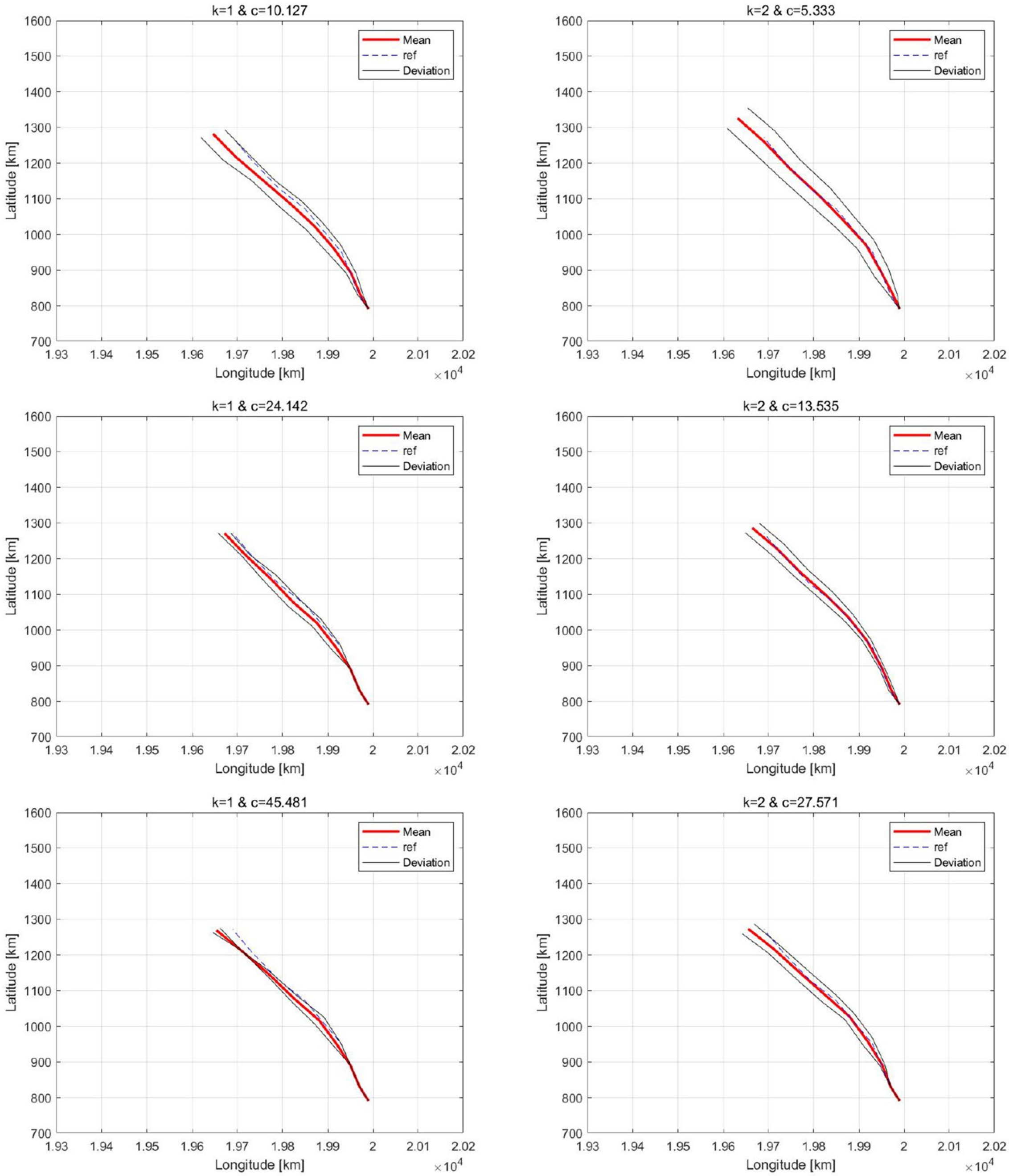

Fig. 18 Same as Fig. 12 but for the MRG wave

typically observed to propagate at roughly 15 m s^{-1} and have synoptic scale wavelength corresponding to wavenumbers in the range $k = 4$ to $k = 10$ (Kiladis et al. 2009). The cases of planetary scale wavenumbers $k = 1, 2$ and slow phase speeds $c = 1, 5$ m s^{-1} can also be deemed to be realistic in the sense that they may be somewhat representative of the Madden Julian Oscillation type wave-disturbance which has comparable phase speeds and wavenumbers and whose zonal structure bears some resemblance to a Kelvin wave disturbance (Kiladis et al. 2009). The case of a Madden-Julian oscillation ought to be investigated on its own because of its importance in tropical atmospheric dynamics (Zhang 2005).

For the Rossby wave case in Figs. 15, 16, 17, the dependence is somewhat reversed compared to the Kelvin wave case. For the small wavenumber cases, $k = 1, 2$ in Fig. 15, there is a large variance in TC trajectories while the mean

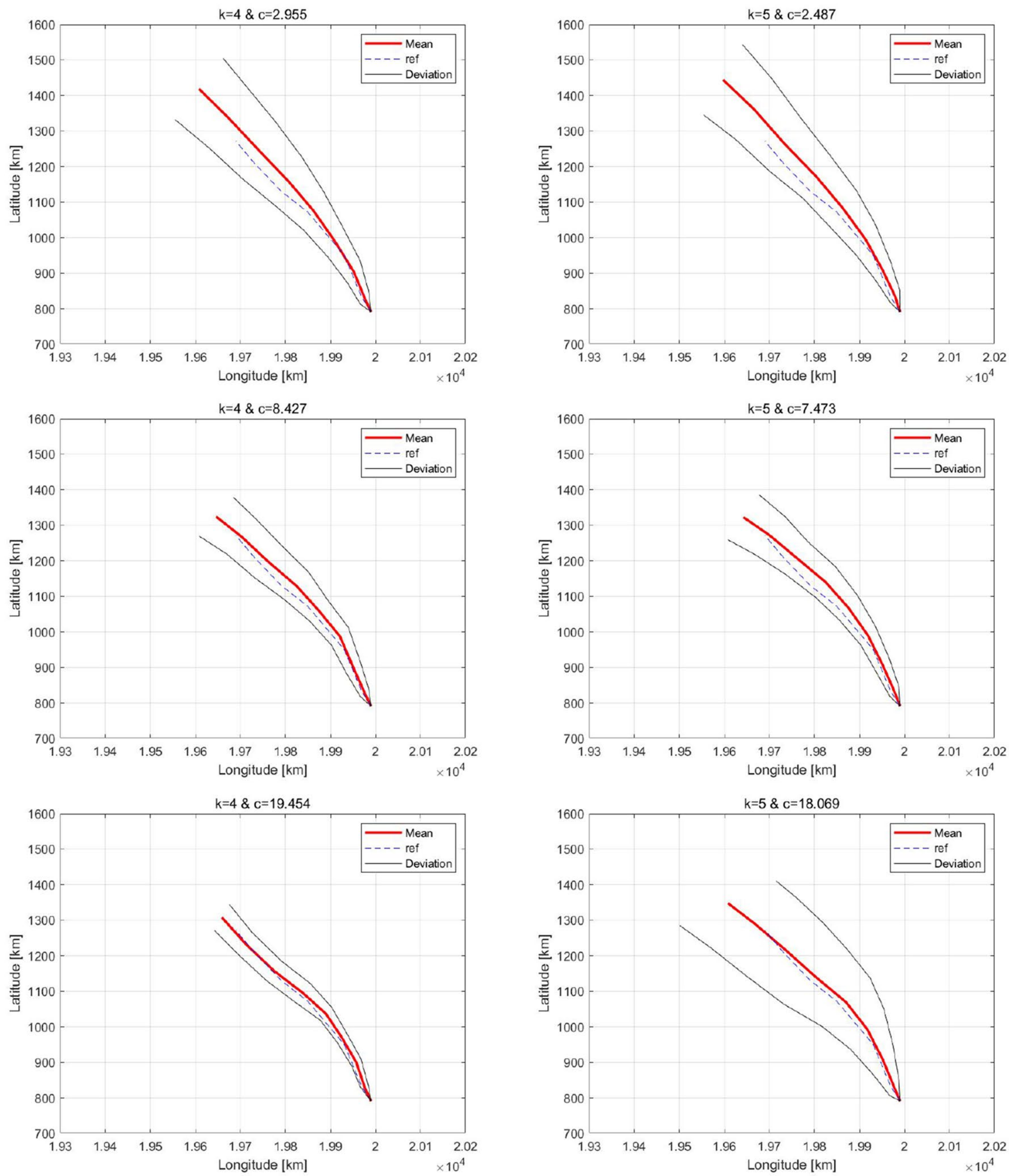

Fig. 19 Same as Fig. 18 but for $k = 4, 5$

path itself seems to depend strongly on the phase speed. For $k = 1$ and $c = -0.332$ m s^{-1} ($c_e = 1$ m s^{-1}), the TC path distribution is severely pulled to the west of the reference trajectory. With $k = 1$ and $c = -1.637$ m s^{-1} ($c_e = 5$ m s^{-1}), we see a somehow similar pattern though the reference path now appears to run along the eastern boundary of the standard deviation cone of trajectories but with $k = 1$ and $c = -4.743$ m s^{-1} ($c_e = 15$ m s^{-1}), the trajectory distribution shifts completely to the east side of the reference path. In all three cases, the mean distance traveled (the mean path arc length) appears to be significantly larger than the reference. For the cases corresponding to $k = 2$ on the right panels, the effect is less dramatic. While we see a somewhat similar effect as in the case $k = 1$ when $c = -0.329$ m s^{-1} ($c_e = 1$ m s^{-1}), the mean path direction is more or less the same as the reference for the two other cases. The variance seems to increase with increasing wavenumber. With the exception of the case $k = 8$ and $c = -1.120$ m s^{-1}

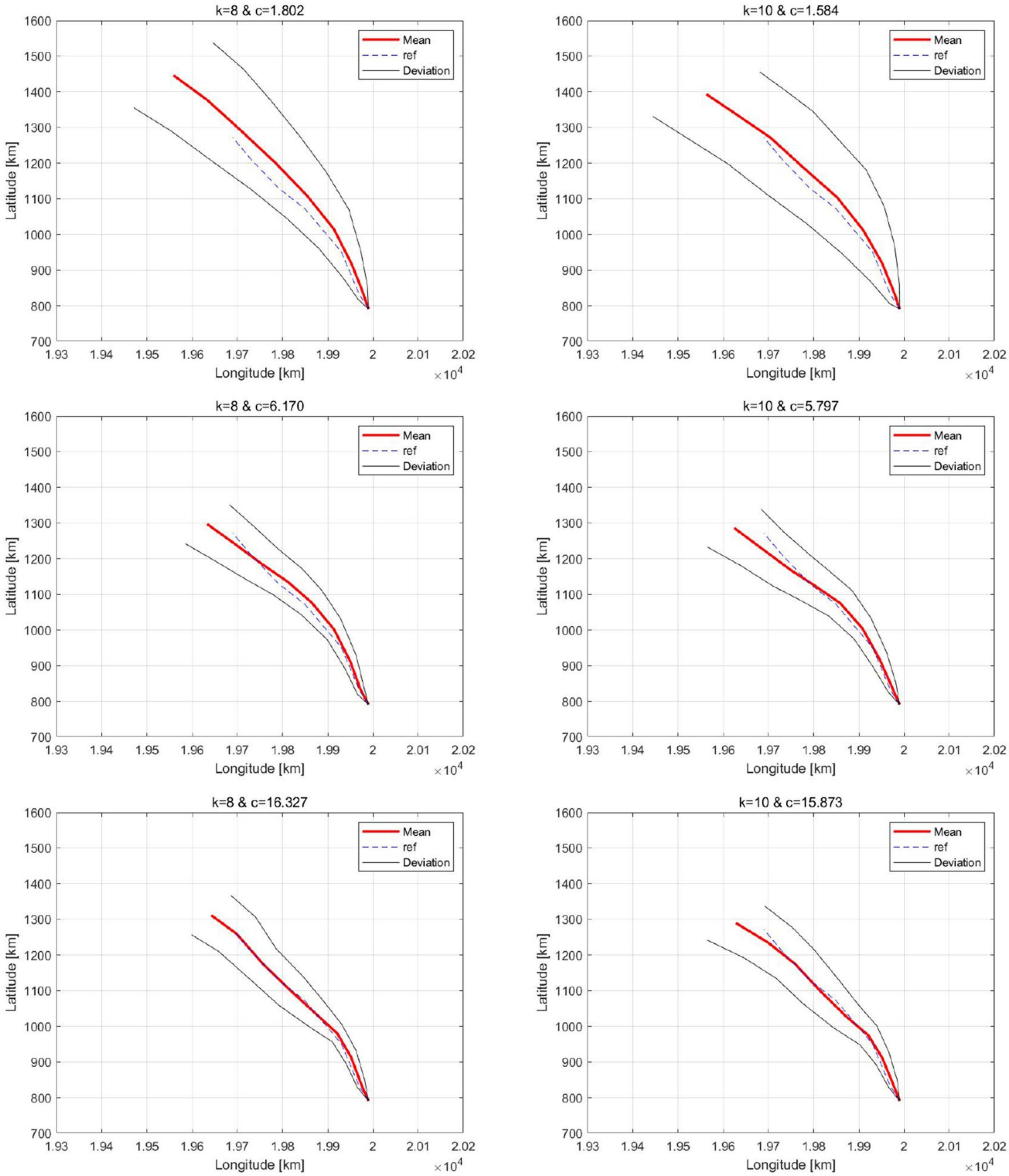

Fig. 20 Same as Fig. 18 but for $k = 8, 10$

on the bottom left of Fig. 17, for all the synoptic scale wavenumber cases, $k = 4, 5, 8, 10$, the effect of the Rossby-wave induced background on the TC trajectory is minimal. Because Rossby waves are mainly planetary scale in nature and appear to move at speeds around -4 m s^{-1} and slower (Kiladis et al. 2009), only the cases in Fig. 15 maybe deemed realistic, as such we can conjecture that in reality Rossby waves may have a stronger impact on TC trajectories compared to Kelvin waves but in both cases, the effect may depend strongly on the wave parameters such as the phase, the phase speed, and the wavenumber.

Somewhat similar to the Kelvin wave case, only Figs. 19 and 20, corresponding on the synoptic scales ($k = 4, 5, 8, 10$), appear to show a significant impact of the MRG wave-induced background on the TC path. The planetary scale cases in Fig. 18 show very little difference between the TC trajectories corresponding to an MRG wave and the reference case, as suggested by the plots of the mean path and associated small variances. Also, as in the Kelvin wave case, the trajectory direction remains stable under the influence of the MRG-induced background while the average distance travelled is however slightly larger than the reference. This is in contrast to the Kelvin wave case which shows a systematically smaller mean distance. From observational point of view, MRG waves move at roughly 20 m s^{-1} and mostly peak at the synoptic scale. It is thus fair to stress that the cases at the bottom in Figs. 19 and 20 are more representative of the real world and may conjecture that MRG waves have in general a small impact on the TC trajectory although some dependance on wave parameters such as phase speed, wavenumber and wave phase are to be expected.

Acknowledgements This research is part of H. S.'s master's thesis. The research of B. K. is partly supported by a Discovery Grant from the Natural Sciences and Engineering Council of Canada.

References

Berner J, Shutts GJ, Leutbecher M, Palmer TN (2009) A spectral stochastic kinetic energy backscatter scheme and its impact on flow-dependent predictability in the ECMWF ensemble prediction system. J Atmos Sci 66:603–626. https://doi.org/10.1175/2008JAS2677.1
Biello J, Majda A (2004) The effect of meridional and vertical shear on the interaction of equatorial baroclinic and barotropic Rossby waves. Stud Appl Math 112:341–390
Chan Johnny C-L, Williams RT (1987) Analytical and numerical studies of the beta-effect in tropical cyclone motion part I: zero mean flow. J Atmos Sci 44(9):1257–1265
Guanghua C, Chia C (2014) Joint contribution of multiple equatorial waves to tropical cyclogenesis over the western north pacific. Mon Weather Rev 142:79–93
Mark D (1985) Tropical cyclone in a nondivergent barotropic model. Mon Weather Rev 113:1199–1210
James F, Boualem K, Maryam N (2009) Two-way interactions between equatorially-trapped waves and the barotropic flow. Chin Ann Math Ser B 30(5):539–568
Fiorino M, Elsberry RL (1989) Some aspects of vortex structure related to tropical cyclone motion. J Atmos Sci 46(7):975–990 (Journal of the Atmospheric Sciences, Vol. 73, pp. 3157–3180)
Frierson DMW, Majda AJ, Pauluis OM (2004) Large scale dynamics of precipitation fronts in the tropical atmosphere: a novel relaxation limit. Commun Math Sci 2:591–626
Huang CY, Chen CA, Chen SH, Nolan D, Upstream track deflection of tropical cyclones past mountain range: Idealized experiments
Hyun-Geun S (2019) Effect of equatorially trapped waves on the tropical cyclone drift. Master Thesis, University of Victoria
Kasahara A, Puri K (1981) Spectral representation of three-dimensional global data by expansion in normal mode functions. Mon Weather Rev 109:37–51
Khouider B (2019) Models for tropical climate dynamics: waves, clouds, and precipitation. Springer, New York
Khouider B, Majda AJ (2000) A non-oscillatory balanced scheme for an idealized tropical climate model Part I: Algorithm and validation. Theoret Comput Fluid Dyn 19(5):355–375
Khouider B, Majda AJ (2005) A non-oscillatory balanced scheme for an idealized tropical climate model Part II: Nonlinear coupling and moisture effects. Theoret Comput Fluid Dyn 19(5):355–375
Khouider B, Majda AJ, Stechmann SN (2013) Climate science in the tropics: waves, vortices and PDEs. Nonlinearity 26(1):R1
Kiladis GN, Wheeler MC, Haertel PT, Straub KH, Roundy PE (2009) Convectively coupled equatorial waves. Rev Geophys 47:2
Li X, Wang W (1994) Barotropic dynamics of the Beta Gyres and Beta drift. J Atmos Sci 51(5):746–756
Majda AJ (2003) Introduction to PDEs and waves for the atmosphere and ocean, vol 9. Courant Lecture Notes in Mathematics. American Mathematical Society, Providence
Majda AJ, Stechmann SN (2009) The skeleton of tropical intraseasonal oscillations. Proc Natl Acad Sci USA 106:8417–8422
Reynolds CA, Doyle James D, Hong X (2016) Examing tropical cyclone-Kelvin wave interactions using adjoint diagnostics. Mon Weather Rev 144:4421–4439
Ross RJ, Kurihara Y (1991) A simplified Scheme to simulate asymmetries due to the beta effect in barotropic vortices. J Atmos Sci 49:1620–1628
Roundy PE (2012) The spectrum of convectively coupled kelvin waves and the madden-julian oscillation in regions of low-level easterly and westerly background flow. J Atmos Sci 69:2107–2111. https://doi.org/10.1175/JAS-D-12-060.1
Roundy PE, Frank WM (2004) A Climatology of waves in the equatorial region. J Atmos Sci 61:2105–2132
Shen B-W (2019) 2019: On the Predictability of 30-day Global Mesoscale Simulations of Multiple African Easterly Waves during summer 2006: a view with a generalized lorenz model. Geosciences 9(7):281. https://doi.org/10.3390/geosciences9070281
Schreck CJ III, Molinari J, Aiyyer A (2012) A global view of equatorial waves and tropical cyclogenesis. Mon Weather Rev 140:774–788
Shen B-W, Tao W-K, Lau WK, Atlas R (2010) Predicting Tropical Cyclogenesis with a Global Mesoscale Model: Hierarchical Multiscale Interactions during the formation of tropical cyclone Nargis (2008). J Geophys Res 115:D14102
Shen B-W, Tao W-K, Wu M-L (2010) African easterly waves in 30-day high-resolution global simulations: a case study during the 2006 NAMMA period. Geophys Res Lett 37:L18803. https://doi.org/10.1029/2010GL044355
Shen B-W, Tao W-K, Lin Y-L, Laing A (2012) Genesis of twin tropical cyclones as revealed by a global mesoscale model: the role of mixed rossby gravity waves. J Geophys Res 117:D13114. https://doi.org/10.1029/2012JD017450
Smith RB (1993) A Hurricane beta-drift law. J Atmos Sci 50:3213–3215
Stern Daniel P, Brisbois James R, Nolan David S (2014) An expanded dataset of hurricane eyewall sizes and slopes. J Atmos Sci 71(7):2747–2762
Wang B, Li X (1992) The beta drift of three-dimensional vortices: a numerical study. Mon Weather Rev 120:579–593
Williams RT, Chan Johnny C-L (1994) Numerical studies of the beta effect in tropical cyclone motion part II: zonal mean flow effect. J Atmos Sci 51(8):1065–1076
Zhao H, Liguang W (2018) Modulation of convectively coupled equatorial Rossby wave on the western north Pacific tropical cyclones activity. Int J Climatol 38:932–948
Zhang C (2005) Madden Julian Oscillation. Rev Geophys 43:RG2003. https://doi.org/10.1029/2004RG000158
Zhou X, Wang B (2007) Transition from an eastern Pacific upper-level mixed Rossby-gravity wave to a western Pacific tropical cyclone. Geophys Res Lett 34:L24801